PHYSICAL REVIEW D **92,** 075004 (2015)

Scrutinizing the alignment limit in two-Higgs-doublet models: $m_h = 125$ GeV

Jérémy Bernon,[1,*] John F. Gunion,[2,†] Howard E. Haber,[3,‡] Yun Jiang,[2,§] and Sabine Kraml[1,¶]

[1]*Laboratoire de Physique Subatomique et de Cosmologie, Université Grenoble-Alpes, CNRS/IN2P3, 53 Avenue des Martyrs, F-38026 Grenoble, France*

[2]*Department of Physics, University of California, Davis, California 95616, USA*

[3]*Santa Cruz Institute for Particle Physics, Santa Cruz, California 95064, USA*

(Received 21 July 2015; published 6 October 2015)

In the alignment limit of a multidoublet Higgs sector, one of the Higgs mass eigenstates aligns with the direction of the scalar field vacuum expectation values, and its couplings approach those of the Standard Model (SM) Higgs boson. We consider *CP*-conserving two-Higgs-doublet models (2HDMs) of Type I and Type II near the alignment limit in which the lighter of the two *CP*-even Higgs bosons, h, is the SM-like state observed at 125 GeV. In particular, we focus on the 2HDM parameter regime where the coupling of h to gauge bosons approaches that of the SM. We review the theoretical structure and analyze the phenomenological implications of the regime of the alignment limit without decoupling, in which the other Higgs scalar masses are not significantly larger than m_h and thus do not decouple from the effective theory at the electroweak scale. For the numerical analysis, we perform scans of the 2HDM parameter space employing the software packages 2HDMC and Lilith, taking into account all relevant pre-LHC constraints, the latest constraints from the measurements of the 125 GeV Higgs signal at the LHC, as well as the most recent limits coming from searches for heavy Higgs-like states. We contrast these results with the alignment limit achieved via the decoupling of heavier scalar states, where h is the only light Higgs scalar. Implications for Run 2 at the LHC, including expectations for observing the other scalar states, are also discussed.

DOI: 10.1103/PhysRevD.92.075004 PACS numbers: 12.60.Fr, 14.80.Bn, 14.80.Ec, 14.80.Fd

I. INTRODUCTION

The minimal version of the Standard Model (SM) contains one complex Higgs doublet, resulting in one physical neutral *CP*-even Higgs boson after electroweak symmetry breaking. The discovery [1,2] of a new particle with mass of about 125 GeV [3] and properties that match very well those expected for a SM Higgs boson was a real triumph of Run 1 of the LHC. Fits of the Higgs couplings performed by ATLAS [4] and CMS [5] show no significant deviations from SM expectations. (A combined global fit of the Higgs couplings based on the Run 1 results was performed by some of us in Ref. [6].) However, one has to keep in mind that the present precisions on the Higgs couplings are, roughly, of the order of tens of percent, so substantial deviations are still possible. Indeed, the SM is not necessarily the ultimate theoretical structure responsible for electroweak symmetry breaking, and theories that go beyond the SM, such as supersymmetry, typically require an extended Higgs sector [7–10]. Hence, the challenge for Run 2 of the LHC, and other future collider programs, is to determine whether the observed state is *the* SM Higgs boson or whether it is part of a nonminimal Higgs sector of a more fundamental theory.

In this paper, we take two-Higgs-doublet models (2HDMs) of Type I and Type II [11] as the prototypes for studying the effects of an extended Higgs sector. Our focus will be on a particularly interesting limit of these models, namely the case in which one of the neutral Higgs mass eigenstates is approximately aligned with the direction of the scalar field vacuum expectation values. In this case, the coupling to gauge bosons of the Higgs boson observed at the LHC tends toward the SM limit, $C_V \to 1$.[1] This so-called *alignment limit* is most easily attained in the decoupling limit [12], where all the other non-SM-like Higgs scalars of the model are heavy. However, the alignment limit of the 2HDM can also be achieved in a parameter regime in which one or more of the non-SM-like Higgs scalars are light (and in some cases very light). This region of *alignment without decoupling* is a primary focus of this paper.

An extensive review of the status of 2HDMs of Type I and Type II was given in Refs. [13,14]. Interpretations of

*bernon@lpsc.in2p3.fr
†jfgunion@ucdavis.edu
‡haber@scipp.ucsc.edu
§yunjiang@ucdavis.edu
¶sabine.kraml@lpsc.in2p3.fr

[1]We use the notation of coupling scale factors, or *reduced couplings*, employed in Ref. [6]: C_V ($V = W, Z$) for the coupling to gauge bosons, $C_{U,D}$ for the couplings to up-type and down-type fermions, and $C_{\gamma,g}$ for the loop-induced couplings to photons and gluons.

1550-7998/2015/92(7)/075004(33)

the recently discovered Higgs boson at 125 GeV in the context of the 2HDMs were also studied in Refs. [15–21]. The possibility of alignment without decoupling was first noted in Ref. [12] and further clarified in Refs. [22,23]. Previous studies of alignment without decoupling scenarios in the light of the LHC Higgs results were conducted in Refs. [24–26]. The specific case of additional light Higgs states in 2HDMs with mass below $\sim 125/2$ GeV was studied in Ref. [27].

Considering experimental as well as theoretical uncertainties, the expected precision for coupling measurements at the LHC after collecting 300 fb^{-1} of data is about 4%–6% for the coupling to gauge bosons and of the level of 6%–13% for the couplings to fermions [28]. The precision improves by roughly a factor of 2 at the high-luminosity run of the LHC with 3000 fb^{-1}. At a future e^+e^- international linear collider (ILC) with $\sqrt{s} = 250$ GeV to 1 TeV, one may measure the couplings to fermions at the percent level and the coupling to gauge bosons at the subpercent level. A detailed discussion of the prospects of various future colliders can be found in Ref. [28].

We take this envisaged $\sim 1\%$ accuracy on C_V as the starting point for the numerical analysis of the alignment case. Concretely, we investigate the parameter spaces of the 2HDMs of Type I and Type II assuming that the observed 125 GeV state is the h, the lighter of the two CP-even Higgs bosons in these models, and imposing that $C_V^h > 0.99$ (note that $|C_V| \leq 1$ in any model of which the Higgs sector consists of only doublets and/or singlets). The case of the heavier CP-even H being the state at 125 GeV will be discussed in a separate paper [29].

Taking into account all relevant theoretical and phenomenological constraints, including the signal strengths of the observed Higgs boson, as well as the most recent limits from the nonobservation of any other Higgs-like states, we then analyze the phenomenological consequences of this scenario. In particular, we study the variations in the couplings to fermions and in the triple-Higgs couplings that are possible as a function of the amount of alignment when the other Higgs states are light and contrast this to what happens in the decoupling regime. Moreover, we study the prospects to discover the additional Higgs states when they are light.

The public tools used in this study include 2HDMC [30] for computing couplings and decay widths and for testing theoretical constraints within the 2HDM context, Lilith 1.1.2 [31] for evaluating the Higgs signal strength constraints, and SusHi-1.3.0 [32] and VBFNLO-2.6.3 [33] for computing production cross sections at the LHC.

The paper is organised as follows. In Sec. II we first review the theoretical structure of the 2HDM. A softly broken discrete $\mathbb{Z}_2$-symmetric scalar potential is introduced using a basis of scalar doublet fields (called the $\mathbb{Z}_2$-basis) in which a the symmetry is manifest. The Higgs basis is then introduced, which provides an elegant framework for exhibiting the alignment limit. We then provide a comprehensive discussion of the Higgs couplings in the alignment regime. In Sec. III, we explain the setup of the numerical analysis and the tools used. The results are presented in Sec. IV. Section V contains our conclusions. In Appendix A, detailed formulas relating the quartic coefficients of the Higgs potential in the $\mathbb{Z}_2$-basis to those of the Higgs basis are given. Some useful analytical expressions regarding the trilinear Higgs self-couplings in terms of physical Higgs masses are collected in Appendix B.

II. *CP*-CONSERVING 2HDM OF TYPES I AND II

In this section, we review the theoretical structure of the two-Higgs-doublet model. Comprehensive reviews of the model can also be found in, e.g., Refs. [12,23,34,35]. To avoid tree-level Higgs-mediated flavor changing neutral currents (FCNCs), we shall impose a Type I or II structure on the Higgs-fermion interactions. This structure can be naturally implemented [36,37] by imposing a discrete $\mathbb{Z}_2$ symmetry on the dimension-4 terms of the Higgs Lagrangian. This discrete symmetry is softly broken by mass terms that appear in the Higgs scalar potential. Nevertheless, the absence of tree-level Higgs-mediated FCNCs is maintained, and FCNC effects generated at one loop are all small enough to be consistent with phenomenological constraints over a significant fraction of the 2HDM parameter space [38–41].

Even with the imposition of the softly broken discrete $\mathbb{Z}_2$ symmetry mentioned above, new CP-violating phenomena in the Higgs sector are still possible, either explicitly due to a physical complex phase that cannot be removed from the scalar potential parameters or spontaneously due to a CP-violating vacuum state. To simplify the analysis in this paper, we shall assume that these CP-violating effects are absent, in which case one can choose a basis of scalar doublet Higgs fields such that all scalar potential parameters and the two neutral Higgs field vacuum expectation values are simultaneously real. Moreover, we assume that only the neutral Higgs fields acquire nonzero vacuum expectation values; i.e., the scalar potential does not admit the possibility of stable charge-breaking minima [42,43].

We first exhibit the Higgs scalar potential, the corresponding Higgs scalar spectrum, and the Higgs-fermion interactions subject to the restrictions discussed above. Motivated by the Higgs data, we then examine the conditions that yield an approximately SM-like Higgs boson.

A. Higgs scalar potential

Let Φ_1 and Φ_2 denote two complex $Y = 1$, $\mathrm{SU}(2)_L$ doublet scalar fields. The most general gauge invariant renormalizable scalar potential is given by

$$\begin{aligned}\mathcal{V} = {} & m_{11}^2\Phi_1^\dagger\Phi_1 + m_{22}^2\Phi_2^\dagger\Phi_2 - [m_{12}^2\Phi_1^\dagger\Phi_2 + \text{H.c.}] \\ & + \frac{1}{2}\lambda_1(\Phi_1^\dagger\Phi_1)^2 + \frac{1}{2}\lambda_2(\Phi_2^\dagger\Phi_2)^2 + \lambda_3(\Phi_1^\dagger\Phi_1)(\Phi_2^\dagger\Phi_2) \\ & + \lambda_4(\Phi_1^\dagger\Phi_2)(\Phi_2^\dagger\Phi_1) + \left\{\frac{1}{2}\lambda_5(\Phi_1^\dagger\Phi_2)^2 + [\lambda_6(\Phi_1^\dagger\Phi_1) \right. \\ & \left. + \lambda_7(\Phi_2^\dagger\Phi_2)]\Phi_1^\dagger\Phi_2 + \text{H.c.}\right\}. \end{aligned} \tag{1}$$

In general, m_{12}^2, λ_5, λ_6, and λ_7 can be complex. As noted above, to avoid tree-level Higgs-mediated FCNCs, we impose a softly broken discrete $\mathbb{Z}_2$ symmetry, $\Phi_1 \to +\Phi_1$, and $\Phi_2 \to -\Phi_2$ on the quartic terms of Eq. (1), which implies that $\lambda_6 = \lambda_7 = 0$, whereas $m_{12}^2 \neq 0$ is allowed. In this basis of scalar doublet fields (denoted as the $\mathbb{Z}_2$-basis), the discrete $\mathbb{Z}_2$ symmetry of the quartic terms of Eq. (1) is manifest. Furthermore, we assume that the scalar fields can be rephased such that m_{12}^2 and λ_5 are both real. The resulting scalar potential is then explicitly CP conserving.

The scalar fields will develop nonzero vacuum expectation values if the Higgs mass matrix m_{ij}^2 has at least one negative eigenvalue. We assume that the parameters of the scalar potential are chosen such that the minimum of the scalar potential respects the $U(1)_{\rm EM}$ gauge symmetry. Then, the scalar field vacuum expectations values are of the form

$$\langle\Phi_1\rangle = \frac{1}{\sqrt{2}}\begin{pmatrix}0\\ v_1\end{pmatrix}, \qquad \langle\Phi_2\rangle = \frac{1}{\sqrt{2}}\begin{pmatrix}0\\ v_2\end{pmatrix}. \tag{2}$$

As noted in Appendix B of Ref. [12], if $|m_{12}^2| \geq \lambda_5|v_1||v_2|$, then the vacuum is CP conserving, and the vacuum expectation values v_1 and v_2 can be chosen to be non-negative without loss of generality. In this case, the corresponding potential minimum conditions are[2]

$$m_{11}^2 = m_{12}^2 t_\beta - \frac{1}{2}v^2(\lambda_1 c_\beta^2 + \lambda_{345}s_\beta^2), \tag{3}$$

$$m_{22}^2 = m_{12}^2 t_\beta^{-1} - \frac{1}{2}v^2(\lambda_2 s_\beta^2 + \lambda_{345}c_\beta^2), \tag{4}$$

where we have defined

$$\lambda_{345} \equiv \lambda_3 + \lambda_4 + \lambda_5, \qquad t_\beta \equiv \tan\beta \equiv \frac{v_2}{v_1}, \tag{5}$$

where $0 \leq \beta \leq \frac{1}{2}\pi$, and

$$v^2 \equiv v_1^2 + v_2^2 = \frac{4m_W^2}{g^2} = (246\ \text{GeV})^2. \tag{6}$$

Of the original eight scalar degrees of freedom, three Goldstone bosons ($G^\pm$ and G) are absorbed ("eaten") by the $W^\pm$ and Z. The remaining five physical Higgs particles are two CP-even scalars (h and H, with $m_h \leq m_H$), one CP-odd scalar (A), and a charged Higgs pair ($H^\pm$). The resulting squared masses for the CP-odd and charged Higgs states are

$$m_A^2 = \bar{m}^2 - \lambda_5 v^2, \tag{7}$$

$$m_{H^\pm}^2 = m_A^2 + \frac{1}{2}v^2(\lambda_5 - \lambda_4), \tag{8}$$

where

$$\bar{m}^2 \equiv \frac{2m_{12}^2}{s_{2\beta}}. \tag{9}$$

The two neutral CP-even Higgs states mix according to the following squared-mass matrix:

$$\mathcal{M}^2 \equiv \begin{pmatrix} \lambda_1 v^2 c_\beta^2 + (m_A^2 + \lambda_5 v^2)s_\beta^2 & [\lambda_{345}v^2 - (m_A^2 + \lambda_5 v^2)]s_\beta c_\beta \\ [\lambda_{345}v^2 - (m_A^2 + \lambda_5 v^2)]s_\beta c_\beta & \lambda_2 v^2 s_\beta^2 + (m_A^2 + \lambda_5 v^2)c_\beta^2 \end{pmatrix}. \tag{10}$$

Defining the physical mass eigenstates

$$H = (\sqrt{2}\text{Re}\Phi_1^0 - v_1)c_\alpha + (\sqrt{2}\text{Re}\Phi_2^0 - v_2)s_\alpha, \tag{11}$$

$$h = -(\sqrt{2}\text{Re}\Phi_1^0 - v_1)s_\alpha + (\sqrt{2}\text{Re}\Phi_2^0 - v_2)c_\alpha, \tag{12}$$

the masses and mixing angle α are found from the diagonalization process

[2]Here and in the following, we use the shorthand notation $c_\beta \equiv \cos\beta$, $s_\beta \equiv \sin\beta$, $c_\alpha \equiv \cos\alpha$, $s_\alpha \equiv \sin\alpha$, $c_{2\beta} \equiv \cos 2\beta$, $s_{2\beta} \equiv \sin 2\beta$, $c_{\beta-\alpha} \equiv \cos(\beta-\alpha)$, $s_{\beta-\alpha} \equiv \sin(\beta-\alpha)$, etc.

$$\begin{pmatrix} m_H^2 & 0 \\ 0 & m_h^2 \end{pmatrix} = \begin{pmatrix} c_\alpha & s_\alpha \\ -s_\alpha & c_\alpha \end{pmatrix}\begin{pmatrix} \mathcal{M}_{11}^2 & \mathcal{M}_{12}^2 \\ \mathcal{M}_{12}^2 & \mathcal{M}_{22}^2 \end{pmatrix}\begin{pmatrix} c_\alpha & -s_\alpha \\ s_\alpha & c_\alpha \end{pmatrix}$$
$$= \begin{pmatrix} \mathcal{M}_{11}^2 c_\alpha^2 + 2\mathcal{M}_{12}^2 c_\alpha s_\alpha + \mathcal{M}_{22}^2 s_\alpha^2 & \mathcal{M}_{12}^2(c_\alpha^2 - s_\alpha^2) + (\mathcal{M}_{22}^2 - \mathcal{M}_{11}^2)s_\alpha c_\alpha \\ \mathcal{M}_{12}^2(c_\alpha^2 - s_\alpha^2) + (\mathcal{M}_{22}^2 - \mathcal{M}_{11}^2)s_\alpha c_\alpha & \mathcal{M}_{11}^2 s_\alpha^2 - 2\mathcal{M}_{12}^2 c_\alpha s_\alpha + \mathcal{M}_{22}^2 c_\alpha^2 \end{pmatrix}. \quad (13)$$

Note that the two equations, $\mathrm{Tr}\mathcal{M}^2 = m_H^2 + m_h^2$ and $\det\mathcal{M}^2 = m_H^2 m_h^2$, yield the following result:

$$|\mathcal{M}_{12}^2| = \sqrt{(m_H^2 - \mathcal{M}_{11}^2)(\mathcal{M}_{11}^2 - m_h^2)}$$
$$= \sqrt{(\mathcal{M}_{22}^2 - m_h^2)(\mathcal{M}_{11}^2 - m_h^2)}. \quad (14)$$

Explicitly, the squared masses of the neutral *CP*-even Higgs bosons are given by

$$m_{H,h}^2 = \frac{1}{2}[\mathcal{M}_{11}^2 + \mathcal{M}_{22}^2 \pm \Delta], \quad (15)$$

where $m_h \le m_H$ and the non-negative quantity Δ is defined by

$$\Delta \equiv \sqrt{(\mathcal{M}_{11}^2 - \mathcal{M}_{22}^2)^2 + 4(\mathcal{M}_{12}^2)^2}. \quad (16)$$

The mixing angle α, which is defined modulo π, is evaluated by setting the off-diagonal elements of the *CP*-even scalar squared-mass matrix given in Eq. (13) to zero. It is often convenient to restrict the range of the mixing angle to $|\alpha| \le \frac{1}{2}\pi$. In this case, c_α is non-negative and is given by

$$c_\alpha = \sqrt{\frac{\Delta + \mathcal{M}_{11}^2 - \mathcal{M}_{22}^2}{2\Delta}} = \sqrt{\frac{\mathcal{M}_{11}^2 - m_h^2}{m_H^2 - m_h^2}}, \quad (17)$$

and the sign of s_α is given by the sign of $\mathcal{M}_{12}^2$. Explicitly, we have

$$s_\alpha = \frac{\sqrt{2}\mathcal{M}_{12}^2}{\sqrt{\Delta(\Delta + \mathcal{M}_{11}^2 - \mathcal{M}_{22}^2)}}$$
$$= \mathrm{sgn}(\mathcal{M}_{12}^2)\sqrt{\frac{m_H^2 - \mathcal{M}_{11}^2}{m_H^2 - m_h^2}}. \quad (18)$$

In deriving Eqs. (17) and (18), we have assumed that $m_h \ne m_H$. The case of $m_h = m_H$ is singular; in this case, the angle α is undefined since any two linearly independent combinations of h and H can serve as the physical states. In the rest of this paper, we shall not consider this mass-degenerate case further.

B. SM limit in the Higgs basis

The scalar potential given in Eq. (1) is expressed in the $\mathbb{Z}_2$-basis of scalar doublet fields in which the $\mathbb{Z}_2$ discrete symmetry of the quartic terms is manifest. It will prove convenient to reexpress the scalar doublet fields in the Higgs basis [44,45], defined by

$$H_1 = \begin{pmatrix} H_1^+ \\ H_1^0 \end{pmatrix} \equiv \Phi_1 c_\beta + \Phi_2 s_\beta,$$
$$H_2 = \begin{pmatrix} H_2^+ \\ H_2^0 \end{pmatrix} \equiv -\Phi_1 s_\beta + \Phi_2 c_\beta, \quad (19)$$

so that $\langle H_1^0 \rangle = v/\sqrt{2}$ and $\langle H_2^0 \rangle = 0$. The scalar doublet H_1 possesses SM tree-level couplings to all the SM particles. Therefore, if one of the *CP*-even neutral Higgs mass eigenstates is SM-like, then it must be approximately aligned with the real part of the neutral field H_1^0.

The scalar potential, when expressed in terms of the doublet fields, H_1 and H_2, has the same form as Eq. (1),

$$\begin{aligned}\mathcal{V} = {} & Y_1 H_1^\dagger H_1 + Y_2 H_2^\dagger H_2 + Y_3[H_1^\dagger H_2 + \mathrm{H.c.}] \\ & + \frac{1}{2}Z_1(H_1^\dagger H_1)^2 + \frac{1}{2}Z_2(H_2^\dagger H_2)^2 + Z_3(H_1^\dagger H_1)(H_2^\dagger H_2) \\ & + Z_4(H_1^\dagger H_2)(H_2^\dagger H_1) + \left\{\frac{1}{2}Z_5(H_1^\dagger H_2)^2 \right. \\ & \left. + [Z_6(H_1^\dagger H_1) + Z_7(H_2^\dagger H_2)]H_1^\dagger H_2 + \mathrm{H.c.}\right\}, \end{aligned} \quad (20)$$

where the Y_i are real linear combinations of the m_{ij}^2 and the Z_i are real linear combinations of the λ_i. In particular, since $\lambda_6 = \lambda_7 = 0$, we have [45,46][3]

$$Z_1 \equiv \lambda_1 c_\beta^4 + \lambda_2 s_\beta^4 + \frac{1}{2}\lambda_{345} s_{2\beta}^2, \quad (21)$$

$$Z_2 \equiv \lambda_1 s_\beta^4 + \lambda_2 c_\beta^4 + \frac{1}{2}\lambda_{345} s_{2\beta}^2, \quad (22)$$

$$Z_i \equiv \frac{1}{4}s_{2\beta}^2[\lambda_1 + \lambda_2 - 2\lambda_{345}] + \lambda_i, \quad (\text{for } i = 3, 4 \text{ or } 5), \quad (23)$$

[3]To make contact with the notation of Ref. [12], $\lambda \equiv Z_1$, $\lambda_V \equiv Z_2$, $\lambda_T \equiv Z_3 + Z_4 - Z_5$, $\lambda_F \equiv Z_5 - Z_4$, $\lambda_A \equiv Z_1 - Z_5$, $\hat{\lambda} \equiv -Z_6$, and $\lambda_U \equiv -Z_7$.

$$Z_6 \equiv -\frac{1}{2}s_{2\beta}[\lambda_1 c_\beta^2 - \lambda_2 s_\beta^2 - \lambda_{345}c_{2\beta}], \tag{24}$$

$$Z_7 \equiv -\frac{1}{2}s_{2\beta}[\lambda_1 s_\beta^2 - \lambda_2 c_\beta^2 + \lambda_{345}c_{2\beta}]. \tag{25}$$

Since there are five nonzero λ_i and seven nonzero Z_i, there must be two relations. The following two identities are satisfied if $\beta \neq 0, \frac{1}{4}\pi, \frac{1}{2}\pi$ [46][4]:

$$Z_2 = Z_1 + 2(Z_6 + Z_7)\cot 2\beta, \tag{26}$$

$$Z_{345} = Z_1 + 2Z_6 \cot 2\beta - (Z_6 - Z_7)\tan 2\beta, \tag{27}$$

where $Z_{345} \equiv Z_3 + Z_4 + Z_5$. One can invert the expressions given in Eqs. (21)–(25), subject to the relations given by Eqs. (26) and (27). The results are given in Appendix A.

The squared mass parameters Y_i are given by

$$Y_1 = m_{11}^2 c_\beta^2 + m_{22}^2 s_\beta^2 - m_{12}^2 s_{2\beta}, \tag{28}$$

$$Y_2 = m_{11}^2 s_\beta^2 + m_{22}^2 c_\beta^2 + m_{12}^2 s_{2\beta}, \tag{29}$$

$$Y_3 = \frac{1}{2}(m_{22}^2 - m_{11}^2)s_{2\beta} - m_{12}^2 c_{2\beta}. \tag{30}$$

Y_1 and Y_3 are fixed by the scalar potential minimum conditions,

$$Y_1 = -\frac{1}{2}Z_1 v^2, \qquad Y_3 = -\frac{1}{2}Z_6 v^2. \tag{31}$$

Using Eqs. (9) and (31), we can express $\bar{m}^2$ in terms of Y_2, Z_1, and Z_6,

$$\bar{m}^2 = Y_2 + \frac{1}{2}Z_1 v^2 + Z_6 v^2 \cot 2\beta. \tag{32}$$

The masses of $H^\pm$ and A are given by

$$m_{H^\pm}^2 = Y_2 + \frac{1}{2}Z_3 v^2, \tag{33}$$

$$m_A^2 = Y_2 + \frac{1}{2}(Z_3 + Z_4 - Z_5)v^2. \tag{34}$$

It is straightforward to compute the CP-even Higgs squared-mass matrix in the Higgs basis [44,47],

$$\mathcal{M}_H^2 = \begin{pmatrix} Z_1 v^2 & Z_6 v^2 \\ Z_6 v^2 & m_A^2 + Z_5 v^2 \end{pmatrix}. \tag{35}$$

[4]For $\beta = 0, \frac{1}{2}\pi$, the $\mathbb{Z}_2$-basis and the Higgs basis coincide, in which case $Z_6 = Z_7 = 0$ and Z_1, Z_2, Z_{345} are independent quantities. For $\beta = \frac{1}{4}\pi$, the two relations are $Z_1 = Z_2$ and $Z_6 = Z_7$, and Z_{345} is an independent quantity.

From Eq. (35), one can immediately derive the conditions that yield a SM-like Higgs boson. Since $\langle H_1^0 \rangle = v/\sqrt{2}$ and $\langle H_2^0 \rangle = 0$, the couplings of H_1 are precisely those of the Standard Model. Thus a SM-like Higgs boson exists if $\sqrt{2}\mathrm{Re}H_1^0 - v$ is an approximate mass eigenstate. That is, the mixing of H_1^0 and H_2^0 is subdominant, which implies that either $|Z_6| \ll 1$ and/or $m_A^2 + Z_5 v^2 \gg Z_1 v^2,\ Z_6 v^2$. Moreover, if in addition $Z_1 v^2 < m_A^2 + Z_5 v^2$, then h is SM-like, whereas if $Z_1 v^2 > m_A^2 + Z_5 v^2$, then H is SM-like. In both cases, the squared mass of the SM-like Higgs boson is approximately equal to $Z_1 v^2$.

The physical mass eigenstates are identified from Eqs. (11), (12), and (19) as

$$H = (\sqrt{2}\mathrm{Re}H_1^0 - v)c_{\beta-\alpha} - \sqrt{2}\mathrm{Re}H_2^0 s_{\beta-\alpha}, \tag{36}$$

$$h = (\sqrt{2}\mathrm{Re}H_1^0 - v)s_{\beta-\alpha} + \sqrt{2}\mathrm{Re}H_2^0 c_{\beta-\alpha}. \tag{37}$$

Then, Eqs. (15) and (16) yield

$$m_{H,h}^2 = \frac{1}{2}[m_A^2 + (Z_1 + Z_5)v^2 \pm \Delta_H], \tag{38}$$

where

$$\Delta_H \equiv \sqrt{[m_A^2 + (Z_5 - Z_1)v^2]^2 + 4Z_6^2 v^4}. \tag{39}$$

In addition, Eq. (14) yields

$$|Z_6|v^2 = \sqrt{(m_H^2 - Z_1 v^2)(Z_1 v^2 - m_h^2)}. \tag{40}$$

Comparing Eqs. (11) and (12) with Eqs. (36) and (37), we identify the corresponding mixing angle by $\alpha - \beta$, which is defined modulo π. Diagonalizing the squared mass matrix, Eq. (35), it is straightforward to derive the following expressions:

$$Z_1 v^2 = m_h^2 s_{\beta-\alpha}^2 + m_H^2 c_{\beta-\alpha}^2, \tag{41}$$

$$Z_6 v^2 = (m_h^2 - m_H^2)s_{\beta-\alpha}c_{\beta-\alpha}, \tag{42}$$

$$m_A^2 + Z_5 v^2 = m_H^2 s_{\beta-\alpha}^2 + m_h^2 c_{\beta-\alpha}^2. \tag{43}$$

It follows that

$$m_h^2 = \left(Z_1 + Z_6 \frac{c_{\beta-\alpha}}{s_{\beta-\alpha}}\right)v^2, \tag{44}$$

$$m_H^2 = m_A^2 + \left(Z_5 - Z_6 \frac{c_{\beta-\alpha}}{s_{\beta-\alpha}}\right)v^2. \tag{45}$$

Note that Eq. (42) implies that[5]

$$Z_6 s_{\beta-\alpha} c_{\beta-\alpha} \le 0. \tag{46}$$

One can also derive expressions for $c_{\beta-\alpha}$ and $s_{\beta-\alpha}$ either directly from Eqs. (41) and (42) or by using Eqs. (17) and (18) with α replaced by $\alpha-\beta$. Using Eq. (46), the sign of the product $s_{\beta-\alpha}c_{\beta-\alpha}$ is fixed by the sign of Z_6. However, since $\beta-\alpha$ is defined only modulo π, we are free to choose a convention where either $c_{\beta-\alpha}$ or $s_{\beta-\alpha}$ is always non-negative.[6] In a convention where $s_{\beta-\alpha}$ is non-negative (this is a convenient choice when the h is SM-like),

$$\begin{aligned} c_{\beta-\alpha} &= -\mathrm{sgn}(Z_6)\sqrt{\frac{Z_1 v^2 - m_h^2}{m_H^2 - m_h^2}} \\ &= \frac{-Z_6 v^2}{\sqrt{(m_H^2 - m_h^2)(m_H^2 - Z_1 v^2)}}, \end{aligned} \tag{47}$$

where we have used Eq. (40) to obtain the second form for $c_{\beta-\alpha}$ in Eq. (47).

Finally, we record the following useful formula that is easily obtained from Eqs. (7) and (A10)[7]:

$$\bar{m}^2 = m_A^2 + Z_5 v^2 + \frac{1}{2}(Z_6 - Z_7)v^2 \tan 2\beta. \tag{48}$$

Combining Eq. (48) with Eqs. (42) and (43) yields

$$\begin{aligned} Z_7 v^2 = {} & (m_h^2 - m_H^2) s_{\beta-\alpha} c_{\beta-\alpha} \\ & + 2\cot 2\beta [m_H^2 s_{\beta-\alpha}^2 + m_h^2 c_{\beta-\alpha}^2 - \bar{m}^2]. \end{aligned} \tag{49}$$

Using Eqs. (26) and (27), one can likewise obtain expressions for $Z_2 v^2$ and $Z_{345} v^2$ in terms of m_h^2, m_H^2, and $\bar{m}^2$. However, these expressions are not particularly illuminating, so we do not write them out explicitly here.

C. Higgs couplings and the alignment limit

As noted in the previous subsection, the Higgs basis field H_1 behaves precisely as the Standard Model Higgs boson. Thus, if one of the neutral CP-even Higgs mass eigenstates is approximately aligned with $\sqrt{2}\mathrm{Re}H_1^0 - v$, then its properties will approximately coincide with those of the SM Higgs boson. Thus, we shall define the alignment limit as the limit in which the one of the two neutral CP-even Higgs mass eigenstates aligns with the direction of the scalar field vacuum expectation values. Defined in this way, it is clear that the alignment limit is independent of the choice of the basis for the two-Higgs-doublet fields. Nevertheless, the alignment limit is most clearly exhibited in the Higgs basis. In light of Eqs. (36) and (37), the alignment limit corresponds either to the limit of $c_{\beta-\alpha} \to 0$ if h is identified as the SM-like Higgs boson or to the limit of $s_{\beta-\alpha} \to 0$ if H is identified as the SM-like Higgs boson.

Consider first the case of a SM-like h, with $m_h \approx 125$ GeV. In this case, $Z_1 v^2 < m_A^2 + Z_5 v^2$, $|c_{\beta-\alpha}| \ll 1$, and $m_h^2 \approx Z_1 v^2$. It follows from Eq. (47) that the alignment limit can be achieved in two ways: (i) $Z_6 \to 0$ or (ii) $m_H \gg v$. The case of $m_H \gg v$ (or equivalently $Y_2 \gg v$) is called the *decoupling limit* in the literature.[8] In this case, one finds that $m_H \sim m_A \sim m_{H^\pm}$, so one can integrate out the heavy scalar states below the scale of m_H. The effective Higgs theory below the scale m_H is a theory with one Higgs doublet and corresponds to the Higgs sector of the Standard Model. Thus, not surprisingly, h is a SM-like Higgs boson. However, it is possible to achieve the alignment limit even if the masses of all scalar states are similar in magnitude in the limit of $Z_6 \to 0$. This is the case of alignment without decoupling and the main focus of this study. Finally, if both $|Z_6| \ll 1$ and $m_H \gg m_h$ are satisfied, the alignment is even more pronounced; when relevant we shall denote this case as the *double decoupling limit*.

For completeness we note that in the case of a SM-like H we have $Z_1 v^2 > m_A^2 + Z_5 v^2$, $|s_{\beta-\alpha}| \ll 1$ and $m_H^2 \approx Z_1 v^2$. Here, it is more convenient to employ a convention where $c_{\beta-\alpha}$ is non-negative. One can then use Eqs. (40), (46), and (47) to obtain an expression for $s_{\beta-\alpha}$. In a convention where $c_{\beta-\alpha}$ is non-negative,

$$\begin{aligned} s_{\beta-\alpha} &= -\mathrm{sgn}(Z_6)\sqrt{\frac{m_H^2 - Z_1 v^2}{m_H^2 - m_h^2}} \\ &= \frac{-Z_6 v^2}{\sqrt{(m_H^2 - m_h^2)(Z_1 v^2 - m_h^2)}}. \end{aligned} \tag{50}$$

Taking $m_H \approx 125$ GeV, there is no decoupling limit as in the case of a SM-like h. However, the alignment limit without decoupling can be achieved in the limit of $Z_6 \to 0$. This case will be discussed in detail in Ref. [29].

We now turn to the tree-level Higgs couplings. Denoting the SM Higgs boson by $h_{\rm SM}$, the coupling of the CP-even

[5]Having established a convention where $0 \le \beta \le \frac{1}{2}\pi$, we are no longer free to redefine the Higgs basis field $H_2 \to -H_2$. Consequently, the sign of Z_6 is meaningful in this convention.

[6]Such a convention, if adopted, would replace the convention employed in Eq. (17) in which c_α is taken to be non-negative.

[7]In Eq. (48), the term in the expression for $\bar{m}^2$ that is proportional to $(Z_6 - Z_7)v^2 \tan 2\beta$ is never greater than $\mathcal{O}(v^2)$ for *all* values of β, since Eqs. (24) and (25) imply that $(Z_6 - Z_7)\tan 2\beta = -\frac{1}{2} s_{2\beta}^2 (\lambda_1 - \lambda_2 - 2\lambda_{345}) \lesssim \mathcal{O}(1)$.

[8]More precisely, we are assuming that $m_H^2 \gg |Z_6| v^2$. Since Z_6 is a dimensionless coefficient in the Higgs basis scalar potential, we are implicitly assuming that Z_6 cannot get too large without spoiling perturbativity and/or unitarity. One might roughly expect $|Z_6| \lesssim 4\pi$, in which case $m_H \gg v$ provides a reasonable indication of the domain of the decoupling limit.

TABLE I. Four possible $\mathbb{Z}_2$ charge assignments that forbid tree-level Higgs-mediated FCNC effects in the 2HDM [48].

	Φ_1	Φ_2	t_R	b_R	τ_R	t_L, b_L, ν_L, e_L
Type I	+	−	−	−	−	+
Type II	+	−	−	+	+	+
Type X (lepton specific)	+	−	−	−	+	+
Type Y (flipped)	+	−	−	+	−	+

Higgs bosons to VV (where $V = W^{\pm}$ or Z) normalized to the $h_{\rm SM}VV$ coupling is given by

$$C_V^h = s_{\beta-\alpha}, \qquad C_V^H = c_{\beta-\alpha}. \tag{51}$$

As expected, if h is a SM-like Higgs boson, then $C_V^h \approx 1$ in the alignment limit, whereas if H is a SM-like Higgs boson, then $C_V^H \approx 1$ in the alignment limit.

Next, we consider the Higgs boson couplings to fermions. The most general renormalizable Yukawa couplings of the two Higgs doublets to a single generation of up- and down-type quarks and leptons (using third-generation notation) is given by

$$\begin{aligned}-\mathcal{L}_{\rm Yuk} = {}& \mathcal{Y}_b^1 \bar{b}_R \Phi_1^i Q_L^i + \mathcal{Y}_b^2 \bar{b}_R \Phi_2^i Q_L^i + \mathcal{Y}_\tau^1 \bar{\tau}_R \Phi_1^i L_L^i \\ & + \mathcal{Y}_\tau^2 \bar{\tau}_R \Phi_2^i L_L^i + \epsilon_{ij}[\mathcal{Y}_t^1 \bar{t}_R Q_L^i \Phi_1^j + \mathcal{Y}_t^2 \bar{t}_R Q_L^i \Phi_2^j] \\ & + \text{H.c.,}\end{aligned} \tag{52}$$

where $\epsilon_{12} = -\epsilon_{21} = 1$, $\epsilon_{11} = \epsilon_{22} = 0$, $Q_L = (t_L, b_L)$, and $L_L = (\nu_L, e_L)$ are the doublet left-handed quark and lepton fields and t_R, b_R, and e_R are the singlet right-handed quark and lepton fields. However, if all terms in Eq. (52) are present, then tree-level Higgs-mediated FCNCs would be present, in conflict with experimental constraints. To avoid tree-level Higgs-mediated FCNCs, we extend the discrete $\mathbb{Z}_2$ symmetry to the Higgs-fermion Lagrangian. There are four possible choices for the transformation properties of the fermions with respect to $\mathbb{Z}_2$, which we exhibit in Table I.

For simplicity, we shall assume in this paper that the pattern of the Higgs couplings to down-type quarks and leptons is the same. This leaves two possible choices for the Higgs-fermion couplings [11]:

$$\text{Type I:}\ \mathcal{Y}_t^1 = \mathcal{Y}_b^1 = \mathcal{Y}_\tau^1 = 0, \tag{53}$$

$$\text{Type II:}\ \mathcal{Y}_t^1 = \mathcal{Y}_b^2 = \mathcal{Y}_\tau^2 = 0. \tag{54}$$

In particular, the pattern of fermion couplings to the neutral Higgs bosons in the Type I and Type II models is exhibited in Table II.

In the strict alignment limit, the fermion couplings to the SM-like Higgs boson should approach their Standard Model values. To see this explicitly, we note the identities,

$$\frac{\cos\alpha}{\sin\beta} = s_{\beta-\alpha} + \cot\beta c_{\beta-\alpha}, \tag{55}$$

$$-\frac{\sin\alpha}{\cos\beta} = s_{\beta-\alpha} - \tan\beta c_{\beta-\alpha}, \tag{56}$$

$$\frac{\sin\alpha}{\sin\beta} = c_{\beta-\alpha} - \cot\beta s_{\beta-\alpha}, \tag{57}$$

$$\frac{\cos\alpha}{\cos\beta} = c_{\beta-\alpha} + \tan\beta s_{\beta-\alpha}. \tag{58}$$

If h is the SM-like Higgs boson, then in the limit of $c_{\beta-\alpha} \to 0$, the fermion couplings of h approach their Standard Model values. However, if $\tan\beta \gg 1$, then the alignment limit is realized in the Type II Yukawa couplings to down-type fermions only if $|c_{\beta-\alpha}|\tan\beta \ll 1$. That is, if $|c_{\beta-\alpha}| \ll 1$ but $|c_{\beta-\alpha}|\tan\beta \sim \mathcal{O}(1)$, then the hVV couplings and the $ht\bar{t}$ couplings are SM-like, whereas the $hb\bar{b}$ and $h\tau^+\tau^-$ couplings deviate from their Standard Model values. Thus, the approach to the alignment limit is *delayed* when $\tan\beta \gg 1$. We denote this phenomenon as the *delayed alignment limit*. Similar considerations apply if $\cot\beta \gg 1$; however, this region of parameter space is disfavored as the corresponding $ht\bar{t}$ coupling quickly becomes nonperturbative if $\cot\beta$ is too large.

Finally, we examine the trilinear Higgs self-couplings. Using the results of Ref. [12] (see also Ref. [47]), the three-Higgs vertex Feynman rules (including the corresponding symmetry factor for identical particles but excluding an overall factor of i) are given by

$$g_{hAA} = -v[(Z_3 + Z_4 - Z_5)s_{\beta-\alpha} + Z_7 c_{\beta-\alpha}], \tag{59}$$

$$g_{HAA} = -v[(Z_3 + Z_4 - Z_5)c_{\beta-\alpha} - Z_7 s_{\beta-\alpha}], \tag{60}$$

TABLE II. Tree-level vector boson couplings C_V ($V = W, Z$) and fermionic couplings C_F normalized to their SM values for the two scalars h, H and the pseudoscalar A in Type I and Type II two-Higgs-doublet models.

	Types I and II	Type I		Type II	
Higgs	VV	Up quarks	Down quarks and leptons	Up quarks	Down quarks and leptons
h	$\sin(\beta-\alpha)$	$\cos\alpha/\sin\beta$	$\cos\alpha/\sin\beta$	$\cos\alpha/\sin\beta$	$-\sin\alpha/\cos\beta$
H	$\cos(\beta-\alpha)$	$\sin\alpha/\sin\beta$	$\sin\alpha/\sin\beta$	$\sin\alpha/\sin\beta$	$\cos\alpha/\cos\beta$
A	0	$\cot\beta$	$-\cot\beta$	$\cot\beta$	$\tan\beta$

$$g_{hHH} = -3v\left[Z_1 s_{\beta-\alpha}c^2_{\beta-\alpha} + Z_{345}s_{\beta-\alpha}\left(\frac{1}{3} - c^2_{\beta-\alpha}\right) + Z_6 c_{\beta-\alpha}(1-3s^2_{\beta-\alpha}) + Z_7 s^2_{\beta-\alpha}c_{\beta-\alpha}\right], \tag{61}$$

$$g_{Hhh} = -3v\left[Z_1 c_{\beta-\alpha}s^2_{\beta-\alpha} + Z_{345}c_{\beta-\alpha}\left(\frac{1}{3} - s^2_{\beta-\alpha}\right) - Z_6 s_{\beta-\alpha}(1-3c^2_{\beta-\alpha}) - Z_7 c^2_{\beta-\alpha}s_{\beta-\alpha}\right], \tag{62}$$

$$g_{hhh} = -3v[Z_1 s^3_{\beta-\alpha} + Z_{345}s_{\beta-\alpha}c^2_{\beta-\alpha} + 3Z_6 c_{\beta-\alpha}s^2_{\beta-\alpha} + Z_7 c^3_{\beta-\alpha}], \tag{63}$$

$$g_{HHH} = -3v[Z_1 c^3_{\beta-\alpha} + Z_{345}c_{\beta-\alpha}s^2_{\beta-\alpha} - 3Z_6 s_{\beta-\alpha}c^2_{\beta-\alpha} - Z_7 s^3_{\beta-\alpha}], \tag{64}$$

$$g_{hH^+H^-} = -v[Z_3 s_{\beta-\alpha} + Z_7 c_{\beta-\alpha}], \tag{65}$$

$$g_{HH^+H^-} = -v[Z_3 c_{\beta-\alpha} - Z_7 s_{\beta-\alpha}]. \tag{66}$$

The trilinear Higgs couplings expressed in terms of the physical Higgs masses are given in Appendix B.

Consider the alignment limit, $c_{\beta-\alpha} \to 0$, where h is SM-like. Then Eqs. (44) and (63) yield[9]

$$g_{hhh} = g^{\rm SM}_{hhh}\left[1 + \frac{2Z_6}{Z_1}c_{\beta-\alpha} + \left(\frac{Z_{345}}{Z_1} - \frac{2Z_6^2}{Z_1^2} - \frac{3}{2}\right)c^2_{\beta-\alpha} + \mathcal{O}(c^3_{\beta-\alpha})\right], \tag{67}$$

where the self-coupling of the SM Higgs boson is given by

$$g^{\rm SM}_{hhh} = -\frac{3m_h^2}{v}. \tag{68}$$

Note that in the alignment limit $m_h^2 \approx Z_1 v^2$ [cf. Eq. (41)], which implies that $Z_1 \approx 0.26$.

It is convenient to make use of Eq. (47) [in a convention where $s_{\beta-\alpha} \geq 0$] to write

$$c_{\beta-\alpha} = -\eta Z_6, \tag{69}$$

where

$$\eta \equiv \frac{v^2}{\sqrt{(m_H^2 - m_h^2)(m_H^2 - Z_1 v^2)}} = \begin{cases} \mathcal{O}(1), & \text{for } m_H^2 \sim \mathcal{O}(v^2), \\ \mathcal{O}\left(\frac{v^2}{m_H^2}\right) \ll 1, & \text{in the decoupling limit.} \end{cases} \tag{70}$$

Inserting Eq. (69) in Eq. (67) yields

$$g_{hhh} = g^{\rm SM}_{hhh}\left\{1 + \left[\left(Z_{345} - \frac{3}{2}Z_1\right)\eta^2 - 2\eta\right]\frac{Z_6^2}{Z_1} + \mathcal{O}(\eta^3 Z_6^3) + \mathcal{O}(\eta^2 Z_6^4)\right\}. \tag{71}$$

In the decoupling limit (where $\eta \ll 1$),

$$g_{hhh} = g^{\rm SM}_{hhh}\left\{1 - \frac{2\eta Z_6^2}{Z_1} + \mathcal{O}(\eta^2 Z_6^2)\right\}. \tag{72}$$

It follows that g_{hhh} is always suppressed with respect to the SM in the decoupling limit.[10] This behavior is confirmed in our numerical analysis. In contrast, in the alignment limit without decoupling, $|Z_6|$ is significantly smaller than 1, and $\eta \sim \mathcal{O}(1)$. It is now convenient to use Eq. (27) to eliminate Z_{345},

$$g_{hhh} = g^{\rm SM}_{hhh}\left\{1 + \left[\left(Z_7\tan 2\beta - \frac{1}{2}Z_1\right)\eta^2 - 2\eta\right]\frac{Z_6^2}{Z_1} + (2\cot 2\beta - \tan 2\beta)\eta^2\frac{Z_6^3}{Z_1} + \mathcal{O}(Z_6^3)\right\}, \tag{73}$$

where the term above designated by $\mathcal{O}(Z_6^3)$ contains no potential enhancements in the limit of $s_{2\beta} \to 0$ or $c_{2\beta} \to 0$. Given that $\eta \sim \mathcal{O}(1)$ in the alignment limit without decoupling, the form of Eq. (73) suggests two ways in which g_{hhh} can be enhanced with respect to the SM. For example if $\tan\beta \sim 1$, then one must satisfy $(Z_7 - Z_6)\eta\tan 2\beta \gtrsim 2 + \frac{1}{2}Z_1\eta$. Alternatively, if $\tan\beta \gg 1$, then one must satisfy $Z_6\eta\cot 2\beta \gtrsim 1 + \frac{1}{4}Z_1\eta$ (the latter inequality requires $Z_6 < 0$, since $\cot 2\beta < 0$ when $\frac{1}{4}\pi < \beta < \frac{1}{2}\pi$). In both cases, $g_{hhh} > g^{\rm SM}_{hhh}$ is possible even when $|Z_6|$ and $|Z_7|$ are significantly smaller than 1. Indeed, both of the above alternatives correspond to $Z_{345} \gg Z_1$ and $\eta Z_{345} \gg 1$ in Eq. (71).

As a second example, consider the hAA coupling given in Eq. (59) [or Eq. (B6)]. Using Eq. (27), we find that in the alignment limit

[9]Equation (67) is obtained in the convention where $s_{\beta-\alpha}$ is non-negative; i.e., $s_{\beta-\alpha}$ is close to 1.

[10]In the double decoupling limit where $\eta \ll 1$ *and* $|Z_6| \ll 1$, Eq. (72) shows that the deviation of g_{hhh} from the corresponding SM value is highly suppressed.

$$g_{hAA} = -\frac{1}{v}\{m_h^2 - 2Z_5 v^2 - (Z_6 - Z_7)v^2 \tan 2\beta + 2Z_6 v^2 \cot 2\beta + \mathcal{O}(c_{\beta-\alpha})\} = -\frac{1}{v}\{m_h^2 - 2\lambda_5 v^2 + 2Z_6 v^2 \cot 2\beta + \mathcal{O}(c_{\beta-\alpha})\} \quad (74)$$

A similar computation yields the Hhh coupling given in Eq. (62) [or Eq. (B11)],

$$g_{Hhh} = \frac{1}{v}\{3Z_6 v^2 - [m_h^2 - 4Z_6 v^2 \cot 2\beta + 2(Z_6 - Z_7)v^2 \tan 2\beta]c_{\beta-\alpha} + \mathcal{O}(c_{\beta-\alpha}^2)\}. \quad (75)$$

In the alignment limit without decoupling, the $\mathcal{O}(1)$ terms in Eqs. (74) and (75) that are proportional to Z_6 should be regarded as terms of $\mathcal{O}(c_{\beta-\alpha})$ [cf. Eqs. (69) and (70)]. That is, the decoupling limit [with $Z_6 \sim \mathcal{O}(1)$] and the alignment limit without decoupling can be distinguished in the trilinear Higgs couplings. Indeed, the Hhh coupling is suppressed in the alignment limit without decoupling, whereas it can be of $\mathcal{O}(v)$ in the decoupling limit. All the other trilinear Higgs self-couplings can be analyzed in the alignment limit following the procedure outlined above.

Last but not least, it is noteworthy that

$$g_{hH^+H^-} = -v[Z_3 + \mathcal{O}(c_{\beta-\alpha})] \quad (76)$$

approaches a finite nonzero value in the alignment limit, with or without decoupling. This is relevant for the analysis of the one-loop process $h \to \gamma\gamma$, which has a contribution that is mediated by an $H^\pm$ loop. In the decoupling limit, the charged Higgs loop amplitude is suppressed by a factor of $\mathcal{O}(v^2/m_{H^\pm}^2)$ relative to the $W^\pm$ and the top quark loop contributions. But, in the alignment limit without decoupling, the charged Higgs loop is parametrically of the same order as the corresponding SM loop contributions, thereby leading to a shift of the $h \to \gamma\gamma$ decay rate from its SM value. This is in stark contrast to the behavior of tree-level Higgs couplings, which approach their SM values in the alignment limit with or without decoupling. That is, the loop-corrected Higgs couplings to SM particles approach their SM values in the decoupling limit but can yield deviations in the alignment limit without decoupling due to internal loops involving light non-SM-like Higgs states.

Before concluding this section, we examine a second theoretical distinction between the decoupling limit and alignment limit without decoupling. The SM Higgs sector is famously unnatural [49,50]. In particular, a fine tuning of the Higgs sector squared-mass parameter is required in order to explain the observed value of the vacuum expectation value (vev), $v \approx 246$ GeV. The 2HDM generically requires two separate and independent fine-tunings. In addition to identifying $v \approx 246$ GeV, which fixes the values of Y_1 and Y_3 in Eq. (31), one must also perform a second fine-tuning to fix the squared-mass parameter Y_2 to be of $\mathcal{O}(v^2)$. Thus, the regime of the decoupling limit (where $Y_2 \gg v^2$) is less fine-tuned than the general 2HDM, since the natural value for Y_2 is the ultraviolet cutoff of the theory beyond which new physics presumably enters. As long as the heavier Higgs scalars (the squared masses of which are of order Y_2) are sufficiently massive, then h will be SM-like.[11]

In contrast, in the case of alignment without decoupling (or in the double decoupling limit), we have $|Z_6| \ll 1$, which is a finely tuned region of the 2HDM parameter space (beyond the two tunings discussed above) unless we can demonstrate that $Z_6 = 0$ is a consequence of an enhanced symmetry of the theory. The possibility of a natural implementation of alignment has been previously treated in Ref. [54]. In the absence of Higgs–fermion Yukawa couplings, it is sufficient to consider the symmetry properties of the scalar potential. Note that we have already imposed a softly broken $\mathbb{Z}_2$ symmetry, which yields $\lambda_6 = \lambda_7 = 0$ in the original basis. In addition, we observe that $Z_6 = Z_7 = 0$ [which also implies that $Y_3 = 0$ in light of Eq. (31)] corresponds to an exact $\mathbb{Z}_2$ symmetry in the Higgs basis.

The conditions $Z_6 = Z_7 = 0$ can be implemented in three ways. If $s_{2\beta} = 0$, then only one of the two Higgs fields acquires a nonzero vev. This means that our original basis and the Higgs basis coincide (in a convention where H_1 denotes the Higgs field with the nonzero vev), in which case the original $\mathbb{Z}_2$ symmetry is unbroken. If $\lambda_6 = \lambda_7 = 0$ and $s_{2\beta}c_{2\beta} \neq 0$, then setting $Z_6 = Z_7 = 0$ in Eqs. (24) and (25) yields $\lambda_1 = \lambda_2 = \lambda_{345}$. Such a scalar potential exhibits a softly broken $CP3$ symmetry, one of the three possible generalized CP symmetries that can be imposed on the 2HDM [55].[12] Finally, if the scalar potential exhibits an exact $CP2$ symmetry, or equivalently there is a basis in which the $\mathbb{Z}_2$ discrete symmetry ($\Phi_1 \to +\Phi_1$, $\Phi_2 \to -\Phi_2$) and a second $\mathbb{Z}_2$ interchange symmetry ($\Phi_1 \leftrightarrow \Phi_2$) coexist [45,55], then it follows that $\lambda_6 = \lambda_7 = 0$, $\lambda_1 = \lambda_2$ (with λ_5 real), $m_{11}^2 = m_{22}^2$, and $m_{12}^2 = 0$. In this case, Eqs. (3) and (4) yield $\tan\beta = 1$.[13] The latter can be maintained when the $CP2$ symmetry is softly broken such that $m_{12}^2 \neq 0$. Using Eqs. (24) and (25) then yields $Z_6 = Z_7 = 0$. Thus, in the

[11] In general, $m_H^2 \gg |Z_6|v^2$ is sufficient to guarantee SM-like h couplings. However, in the 2HDM with Type II Yukawa coupling and $\tan\beta > 1$, a SM-like h coupling to down-type quarks and leptons requires $m_H^2 \gg |Z_6|v^2 \tan\beta$, leading to the phenomenon of delayed decoupling [12,51–53] at large $\tan\beta$. This is a special case of delayed alignment introduced below Eq. (58).

[12] If $m_{12}^2 = 0$ in Eq. (1) in addition to $\lambda_6 = \lambda_7 = 0$, then the $\mathbb{Z}_2$ discrete symmetry ($\Phi_1 \to +\Phi_1$, $\Phi_2 \to -\Phi_2$) is exact. In this case, $Z_6 = Z_7 = 0$ implies that $\lambda_1 = \lambda_2 = \lambda_{345}$ *and* $m_{11}^2 = m_{22}^2$ [the latter via Eq. (30)] and corresponds to an *exact* $CP3$ symmetry of the scalar potential. This restriction of scalar potential parameters has also been obtained in Ref. [54].

[13] Here we assume that $\lambda_1 \neq \lambda_{345}$; otherwise, the $CP2$ symmetry is promoted to the $CP3$ symmetry previously considered.

absence of the Higgs-fermion Yukawa couplings, $Z_6 = 0$ is a consequence of an enhanced symmetry of the scalar potential, in which case the regime of alignment without decoupling and the double decoupling regime are both natural in the sense of 't Hooft [56].

If we now include the Higgs-fermion Yukawa coupling, we can still maintain the symmetry of the scalar potential in special cases. If the $\mathbb{Z}_2$ symmetry transformation is defined in the Higgs basis such that H_2 is odd (i.e., $H_2 \to -H_2$) and H_1 and all fermion and vector fields are even, then the resulting model corresponds to a Type I 2HDM with $s_{2\beta} = 0$, which we recognize as the inert 2HDM [57,58]. Indeed, if we perturb the inert 2HDM by taking Z_6 and Z_7 small, then either h or H will be approximately SM-like. In the case of $s_{2\beta} \neq 0$, we would need to extend the (softly broken) $CP3$ or $CP2$ symmetry of the scalar potential to the Higgs-fermion Yukawa sector. As shown in Ref. [59], no phenomenologically acceptable $CP2$-symmetric model exists. A unique softly broken $CP3$-symmetric 2HDM does exist with an acceptable fermion mass spectrum; however, this model does not appear to be phenomenologically viable due to insufficient CP violation and potentially large FCNC effects [59]. Hence, for generic choices of the 2HDM parameters, the regime of alignment without decoupling and the double decoupling regime must be regarded as more finely tuned than the generic 2HDM.

III. SETUP OF THE NUMERICAL ANALYSIS

In this section, we give details on the numerical procedure. In particular, we describe the scan of the 2HDM parameter space and the different constraints coming from theoretical requirements, signal strengths of the observed 125 GeV Higgs state, flavor physics, and direct searches for extra Higgs states.

Imposing a softly broken $\mathbb{Z}_2$ symmetry ($\Phi_1 \to +\Phi_1$, $\Phi_2 \to -\Phi_2$) on the scalar potential given in Eq. (1) which sets $\lambda_6 = \lambda_7 = 0$, the free parameters of the 2HDM scalar potential can be chosen to be the four physical Higgs masses $m_h, m_H, m_{H^\pm}, m_A$; the mass term m_{12}^2; the ratio of the two Higgs vacuum expectation values $\tan\beta$; and the mixing angle α of the CP-even Higgs squared-mass matrix. In this study, we choose the following ranges for the scan:

$$\begin{aligned} &\alpha \in [-\pi/2, \pi/2], \quad \tan\beta \in [0.5, 60], \\ &m_{12}^2 \in [-(2000\ \mathrm{GeV})^2, (2000\ \mathrm{GeV})^2], \\ &m_{H^\pm} \in [m^*, 2000\ \mathrm{GeV}], \quad m_A \in [5\ \mathrm{GeV}, 2000\ \mathrm{GeV}], \end{aligned} \tag{77}$$

where m^* is a lower bound on the charged Higgs mass originating either from the LEP direct searches [60] or constraints from B-physics, mainly from the $Z \to b\bar{b}$ (R_b), $\epsilon_K, \Delta m_{B_s}$, $B \to X_s\gamma$, and $B \to \tau\nu$ constraints [38–41]. In principle, both h and H can have the same properties as the SM Higgs and thus serve as possible candidates for the observed SM-like Higgs state. In this paper, we consider $m_h \equiv 125.5$ GeV,[14] taking

$$m_H \in [129.5\ \mathrm{GeV}, 2000\ \mathrm{GeV}]. \tag{78}$$

As mentioned in Sec. II A, the degenerate case $m_h \approx m_H$ is not considered in this study. Instead, we require a 4 GeV mass splitting between h and H in order to avoid H contamination of the h signal. Since we are primarily interested in the case that the electroweak gauge bosons acquire most of their masses from only one of the Higgs basis doublet fields, we impose $s_{\beta-\alpha} \geq 0.99$, which translates into $|c_{\beta-\alpha}| \lesssim 0.14$. This implies that we are allowing at most a 1% deviation from $C_V^h = 1$. This should be compared with the expected ultimate precision for C_V of about 2%–4% at the high-luminosity LHC and about 0.2%–0.5% at the ILC [23,28].

We perform a flat random scan over this parameter space using the public code 2HDMC [30] for a precise state-of-the-art computation of the couplings and decay widths of the various Higgs states. Only points satisfying the stability of the scalar potential [cf. Eq. (A17)], coupling perturbativity, and tree-level S-matrix unitarity are retained. We also require the S, T, and U Peskin–Takeuchi parameters [61] to be compatible with their corresponding values derived from electroweak precision observables [62]. These constraints are also checked by means of 2HDMC.

Next we impose constraints from the nonobservation of Higgs states other than the one at 125 GeV. From the LEP direct searches for light Higgs states, we consider the cross section upper limits on $e^+e^- \to Zh/H$ and $e^+e^- \to Ah/H$ from Refs. [63] and [64], respectively. For very light A below 9.5 GeV, the limits from Upsilon decays [65] are important, for which we follow the implementation in NMSSMTools 4.6.0 [66]. Moreover, we consider the limits from CMS on light pseudoscalars decaying into $\mu^+\mu^-$ [67] in the mass ranges $m_A = 5.5$–9 and 11.5–14 GeV, which are relevant in particular in Type II models. The limits from LHC searches for additional heavy Higgs states are also taken into account. These include the model-independent limits from the searches for $H \to ZZ^{(*)} \to 4\ell$ from ATLAS [68] and CMS [69] and for $H \to ZZ^{(*)} \to 2\ell 2\nu$ from CMS [70]. However, these limits are easily evaded in our study where it is the h that has $C_V^h = s_{\beta-\alpha} > 0.99$, while HVV couplings behave as $c_{\beta-\alpha}$ and $|c_{\beta-\alpha}| \leq 0.14$. (This also holds true in view of the Moriond 2015 update of the Higgs data [71].) More important are the limits from $H, A \to \tau\tau$ searches in gluon-fusion or associated production with a pair of b quarks from ATLAS [72] and CMS [73]. These are particularly relevant in the large $\tan\beta$ region of the Type

[14]Having performed the parameter scans before the publication of Ref. [3] which reports a central value of the Higgs mass of 125.09 GeV, we use 125.5 GeV as the observed Higgs mass in this analysis.

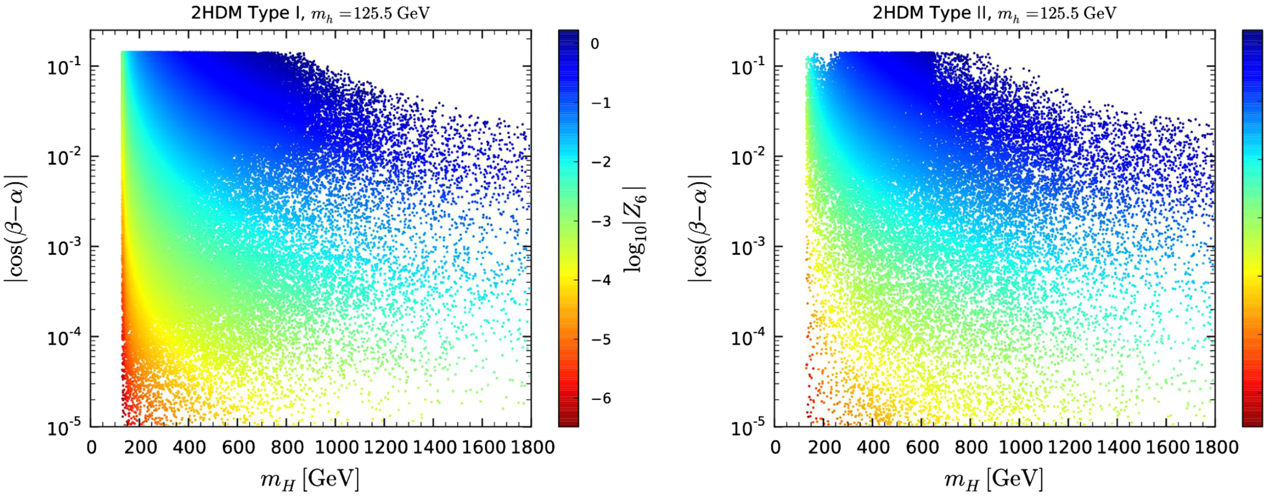

FIG. 1 (color online). $|c_{\beta-\alpha}|$ vs m_H in Type I (left) and Type II (right) with $\log_{10}|Z_6|$ color code. Points are ordered from high to low $\log_{10}|Z_6|$ values.

II models where a significant enhancement of the down-type fermion coupling to the neutral Higgs states occurs. Finally, the limits derived from the pseudoscalar search $A \to Zh, h \to b\bar{b}$ from ATLAS [74] and CMS [75] are imposed. (Limits from other searches, like for $A \to Z\gamma$ [76] or $hh \to b\bar{b}b\bar{b}$ [77], have no effect on the results; the very recent CMS limits on $A \to ZH$ and $H \to ZA$ [78] are not taken into account but will be commented upon in Sec. IV D.) To evaluate all these constraints, production of the H and A via gluon-gluon fusion (ggF) and via associated production with a pair of bottom quarks (bbH,bbA) are computed at next-to-next-to-leading-order (NNLO) QCD[15] accuracy using SusHi-1.3.0 [32], while the vector-boson fusion (VBF) mode for the H is computed at next-to-leading order (NLO) with VBFNLO-2.6.3 [33].

Signal strengths constraints coming from the precise measurements of the properties of the 125 GeV state are taken into account by means of Lilith 1.1.2 [31]. We require each point of the analysis to be allowed at the 95% C.L. The C.L. is derived from the log-likelihood ratio

$$\Delta(-2\ln L)(\mathcal{P}) = -2\ln L(\mathcal{P}/\widehat{2\mathrm{HDM}}), \tag{79}$$

where L is the likelihood constructed by Lilith using up-to-date signal strength measurements, $\mathcal{P}$ represents the set of parameters of the tested point, and $\widehat{2\mathrm{HDM}}$ the best-fit point of the model. The Lilith database 15.04 is used for this analysis. It contains all the latest Higgs signal strengths measurements from ATLAS [4,79–87] and CMS [5,69,88–94] as of April 2015 and a combined D0 and CDF result [95].

[15]The NNLO corrections for ggF are only computed for the top quark loop, as those for the bottom quark loop are very small.

IV. RESULTS

A. Parameters

Let us start by reviewing the relevant parameter space. Figure 1 shows the crucial relation between $|Z_6|$, $|c_{\beta-\alpha}|$, and m_H, illustrating the different ways alignment can occur with and without decoupling.[16] As expected, $|Z_6|$ exhibits a clear dependence on the $H-h$ mass difference, see Eq. (42), and steeply drops toward zero in the limit $|c_{\beta-\alpha}| \to 0$, i.e. when the h becomes purely SM-like. When m_H is of the order of 1 TeV, one needs to be extremely close to $s_{\beta-\alpha} = 1$ to have small $|Z_6|$—for instance $|Z_6| \approx 10^{-3}$ requires $|c_{\beta-\alpha}| \approx 6 \times 10^{-5}$ for $m_H = 1$ TeV. In constrast, for a lighter H, the departure of $s_{\beta-\alpha}$ from 1 can be more important—for instance the same $|Z_6| \approx 10^{-3}$ value requires $|c_{\beta-\alpha}| \approx 2 \times 10^{-3}$ for $m_H = 200$ GeV. It is in principle always possible to obtain arbitrarily small values of $|Z_6|$ if one pushes $s_{\beta-\alpha}$ arbitrarily close to 1. For the purpose of the numerical analysis, we limit ourselves to $|c_{\beta-\alpha}| \geq 10^{-5}$; we have checked that this captures well all features relevant for the $|c_{\beta-\alpha}| \to 0$ limit. Interestingly, as m_H becomes larger, we observe that the decoupling limit sets a stronger upper limit on $|c_{\beta-\alpha}|$ than the one set in the numerical scan ($|c_{\beta-\alpha}| \lesssim 0.14$). Observing

[16]In this and subsequent figures, we give 3D information on a 2D plot by means of a color code in the third dimension. To this end, we must chose a definite plotting order. Ordering the points from high to low values in the third dimension, as done for $\log_{10}|Z_6|$ in Fig. 1, means that the highest values are plotted first and lower and lower values are plotted on top of them. As a consequence, regions with low values may (partly) cover regions with high values. The opposite is of course true for the ordering from low to high values. To avoid a proliferation of plots, in each figure, we show only one ordering, trying to choose the one that gives most information. The figures with inverted plotting order are available upon request.

a heavy $m_H \gtrsim 850$ GeV at the LHC would provide a better-than-1% indirect determination of the h-coupling to electroweak gauge bosons in the framework of these scenarios.

The range of m_A is also interesting. In principle, m_A can be above or below $m_{h,H}$, and even $m_A < m_h/2$ is possible and consistent with the data [27]. However, once m_H is fixed, the allowed range of m_A is limited (and vice versa) as illustrated in Fig. 2. We see that in both Type I and Type II, if the scalar H is heavy and decoupled, the same is true for the pseudoscalar A. Conversely, if m_H is light, say below 600 GeV, also m_A must be below about 800 GeV. Furthermore, it appears that for $|c_{\beta-\alpha}| \lesssim 10^{-3}$ (or, equivalently, small $|Z_6|$) $m_H < m_A$ is favored. This can be understood from Eq. (43) [or Eq. (45)]: since the $m_h^2 c_{\beta-\alpha}^2$ (or $Z_6 c_{\beta-\alpha}/s_{\beta-\alpha}$) term therein is always quite small, the mass ordering between m_H and m_A is largely determined by the sign of Z_5. The value of Z_5, in turn, is driven by λ_5 [cf. Eq. (A13)], which according to our numerical analysis tends to be negative for small $c_{\beta-\alpha}$.

A strong interrelation is also found between m_A, m_H, and $m_{H^\pm}$ as illustrated in Fig. 3. The two panels show m_H vs m_A with color coding according to $m_{H^\pm}$, with the ordering going from high (blue) to low (red) $m_{H^\pm}$ values. While the correlation of $m_{H^\pm}$ with m_H and m_A is somewhat different in Type I and Type II, in both models, a light charged Higgs below 500–600 GeV requires that the H and A also be not too heavy, with masses below about 800 GeV. When inverting the plotting order of $m_{H^\pm}$ (not shown), we find that for any given $m_{H^\pm}$ there is a lower limit on m_H and

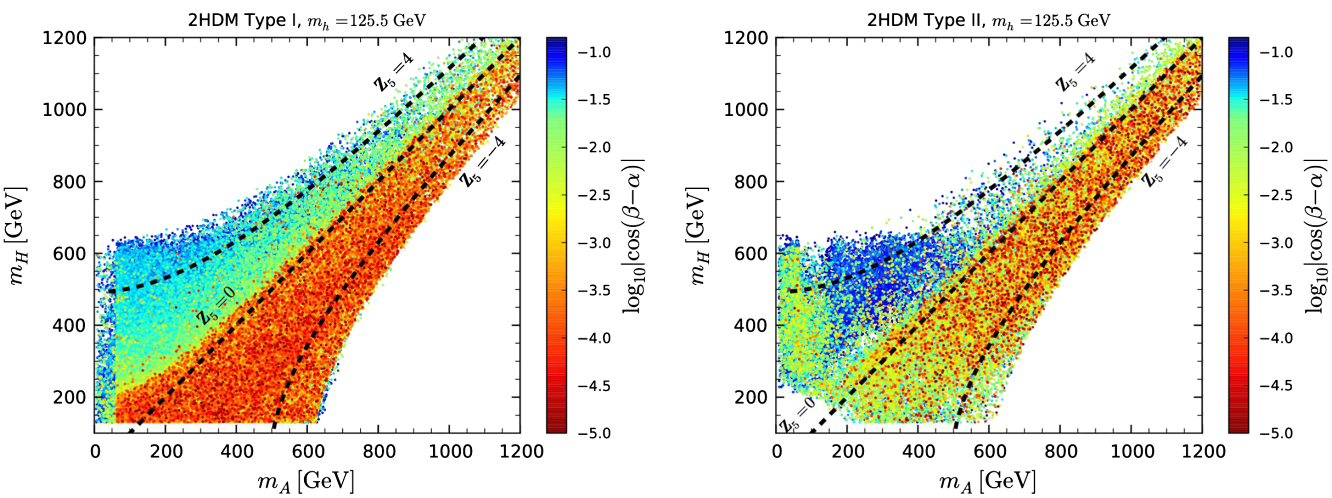

FIG. 2 (color online). m_H vs m_A in Type I (left) and Type II (right) with the color code indicating the value of $\log_{10}|c_{\beta-\alpha}|$. Points are ordered from high to low $\log_{10}|c_{\beta-\alpha}|$. The dashed lines are isolines of $Z_5 = 4$ (upper line), 0 (middle line), and −4 (lower line) for $|c_{\beta-\alpha}| = 0.015$ (varying $|c_{\beta-\alpha}|$ from 0 to 0.14 has no visible effect on them).

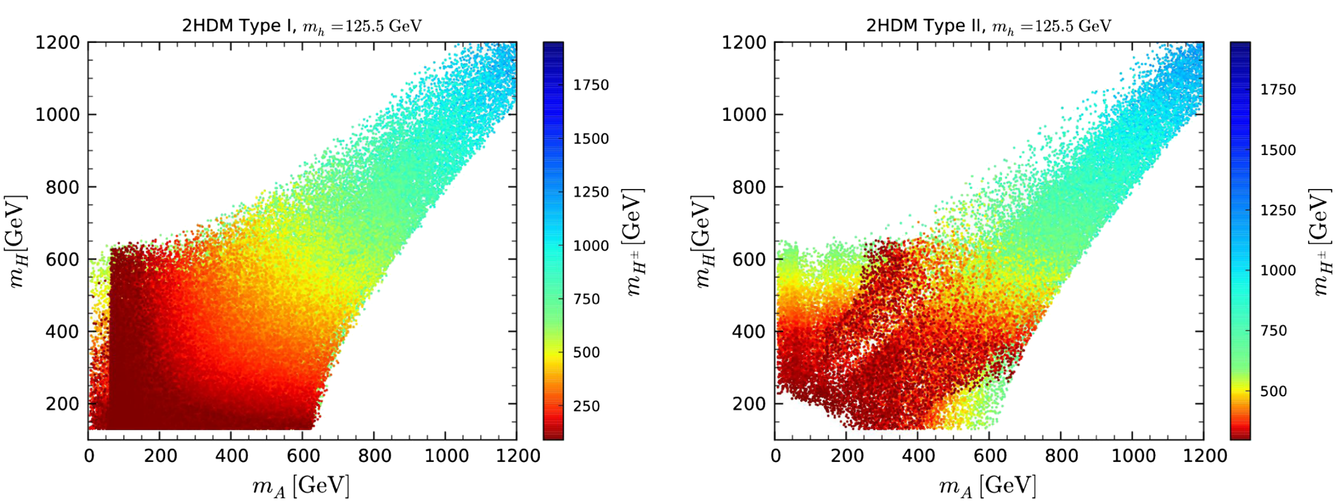

FIG. 3 (color online). m_H vs m_A in Type I (left) and Type II (right) with the color code indicating the value of $m_{H^\pm}$. Points are ordered from high to low $m_{H^\pm}$.

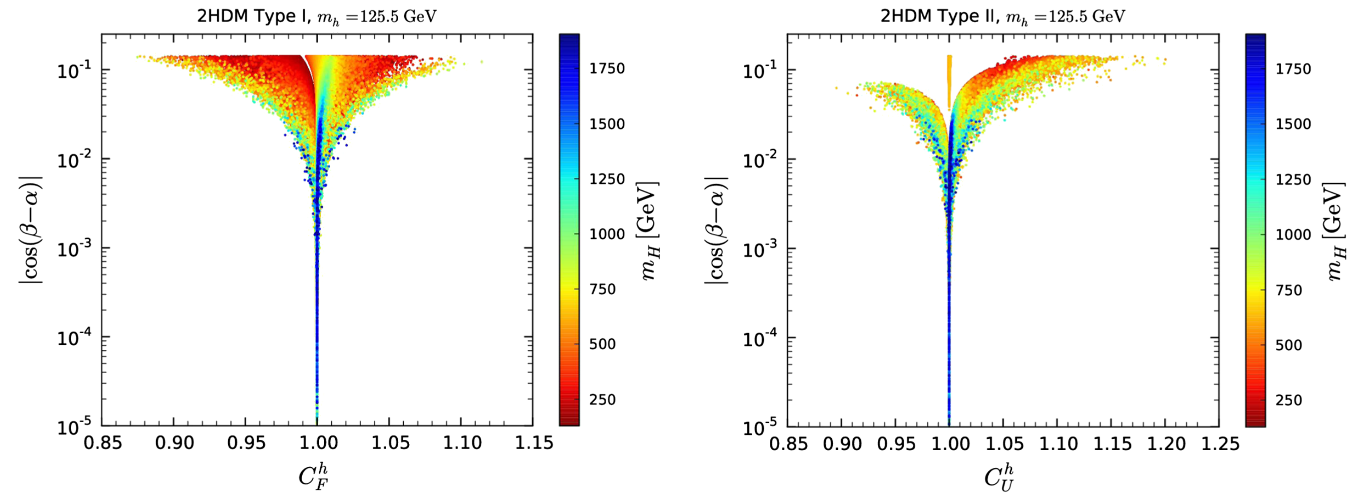

FIG. 4 (color online). $|c_{\beta-\alpha}|$ vs C_F^h in Type I (left) and $|c_{\beta-\alpha}|$ vs C_U^h in Type II (right) with m_H color code. Points are ordered from low to high m_H. The points with $C_U^h \approx 1$ and $|c_{\beta-\alpha}| > 0.03$ are the points for which $C_D^h \approx -1$, i.e., the opposite-sign Yukawa coupling points; see Fig. 5.

m_A: for $m_{H^\pm} \sim 1$ TeV, also $m_{H,A}$ are of that order. In turn, when m_H and m_A are in the nondecoupling regime, $m_{H^\pm}$ cannot be much heavier. The absence of points in a triangular region at low m_A and m_H in Type II (but not for Type I) is due to the fact that in the Type II model B-physics requires $m_{H^\pm} \gtrsim 300$ GeV and at low m_A the precision electroweak T parameter constraint would be violated if m_H differs very much from $m_{H^\pm}$.[17]

B. Couplings

The next question to address is what variations in the couplings of the 125.5 GeV state are still possible in the limit of approximate alignment where $C_V^h \approx 1$. In particular, recall that in the scan we impose $s_{\beta-\alpha} > 0.99$ with $m_h = 125.5$ GeV, without requiring, however, that the other couplings of the h be very SM-like. To answer this question, we first show in Fig. 4 the dependence of the reduced couplings to (up-type) fermions, see Table II, $C_F^h \equiv C_U^h = C_D^h$ in Type I (C_U^h in Type II) on $|c_{\beta-\alpha}|$. The mass of the heavier scalar H is shown as a color code. We see that when m_H is light, for only 1% deviation from unity in C_V^h, C_U^h can deviate as much as about 10% (20%) from unity in Type I (Type II). Inverting the plotting order of m_H (not shown), it is interesting to note that these deviations are largest for $m_H \approx 700$–800 GeV while slightly more constrained for lighter m_H. On the other hand, in the decoupling limit, the deviations in C_U^h are more constrained, with a maximum of 5% for $m_H \gtrsim 1.2$ TeV in both Type I and Type II. It is also interesting to observe how quickly alignment leads to SM-like couplings: for $|c_{\beta-\alpha}| \lesssim 10^{-2}$, the deviations in C_U^h are limited to just a few percent no matter the value of m_H.

The situation is quite different for the coupling to down-type fermions, C_D^h, in Type II, see Fig. 5. First of all, the possible deviations are larger than for C_U^h, with C_D^h ranging from about 0.70 to 1.15 even for $|c_{\beta-\alpha}| \sim 10^{-2}$. Indeed, this is an example of the delayed alignment limit discussed below Eq. (58); one needs $|c_{\beta-\alpha}|$ as low as about 3×10^{-4} to have C_D^h within 2% of unity. This drives the whole phenomenology of the scenario: as we will see, sizable deviations of C_D^h from 1 lead to possible large deviations in the signal strengths even for quite small $|c_{\beta-\alpha}|$. Inverting the plotting order of m_H (not shown), we note, however, that for any given $|c_{\beta-\alpha}|$ of a few times 10^{-3} or smaller C_D^h is limited to be closer to 1 when m_H is small than in the decoupling case with large m_H.

Moreover, $C_D^h = 1$ is not possible unless $|c_{\beta-\alpha}|$ is very small (again a few times 10^{-3} or smaller). In particular, large positive deviations of $C_D^h \gtrsim 1.12$ would indicate $m_H \lesssim 750$ GeV. On the contrary, C_D^h values which are substantially smaller than 1 can be achieved in both the decoupling and nondecoupling regimes except for a small island of points located around $C_D^h \approx 0.8$ and $|c_{\beta-\alpha}| \approx 0.1$ that is achieved only for $m_H \lesssim 400$ GeV. Thus, a discovery of a light H state in association with a measured value of $C_D^h \sim 0.8$ would give an indirect way to probe subpercent deviation of C_V^h in this Type II scenario.

Finally, for light m_H, the sign of C_D^h relative to C_V^h and C_U^h can be opposite to the corresponding SM value. This is realized for not so small values of $|c_{\beta-\alpha}| \geq 0.035$, i.e. not in the deep alignment limit, for 230 GeV $\leq m_H \leq 665$ GeV, $m_A \lesssim 650$ GeV, and $0.08 \leq |Z_6| \leq 0.92$. For the points in

[17] Very recently, the analysis of Misiak and collaborators [96] has improved the charged Higgs mass bound in the Type II 2HDM to $m_{H^\pm} \gtrsim 480$ GeV at 95% C.L. We have not implemented this stricter bound in our scans.

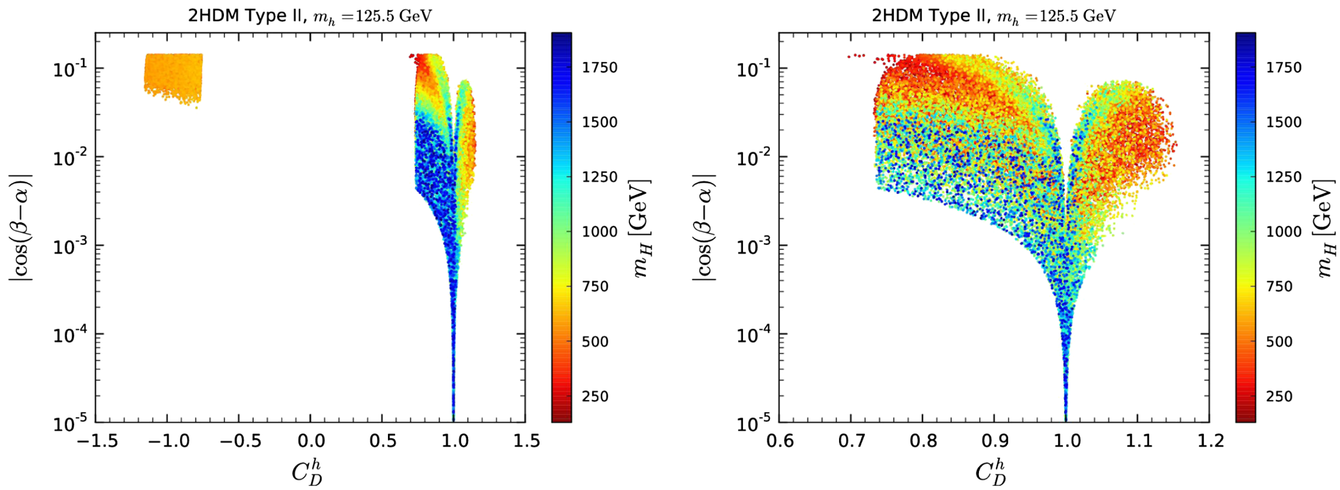

FIG. 5 (color online). $|c_{\beta-\alpha}|$ vs C_D^h in Type II with the m_H color code for the full C_D^h range (left) and zooming in on the $C_D^h > 0$ region (right). Points are ordered from low to high m_H.

this region, the up-type coupling is very close to 1, corresponding to the few isolated points observed in the right panel of Fig. 4. As discussed in Ref. [53], the eventual LHC Run 2 precision will allow one to either confirm or eliminate the opposite-sign coupling possibility using precise signal rate measurements of the h in a few channels. Should the opposite-sign coupling be confirmed, one would expect to also see A signals (plus perhaps H signals) in the above mass range, thereby providing a confirmation of this scenario. (The cross sections for A and H signals will be discussed in Sec. IV D.)

The $\tan\beta$ dependence of the fermion couplings of h is shown in Fig. 6. We see that large $\tan\beta$ leads to C_F^h very close to 1 in Type I and C_U^h very close to 1 in Type II. However, in Type II, at large $\tan\beta$, small $c_{\beta-\alpha}$ is not enough to drive $C_D^h \to 1$: the approach to SM-like coupling is delayed, as discussed in Sec. II in the text below Table II. Note also that the opposite-sign C_D^h solution in Type II requires $\tan\beta \gtrsim 10$ and $C_V^h \sim 0.9994$ (which is experimentally indistinguishable from exact alignment).

The loop-induced coupling to photons, C_γ^h, is presented in Fig. 7. Even at very small $c_{\beta-\alpha}$, C_γ^h can deviate substantially from 1. This is due to the charged-Higgs contribution to the $h\gamma\gamma$ coupling. This contribution can be large with either sign, positive or negative, in Type I, while in Type II, *large* contributions are always negative and suppress C_γ^h [53]. Note in particular the Type II points with $C_\gamma^h \sim 0.95$ associated with the opposite-sign C_D^h cases for which the charged Higgs loop contribution does not decouple and always leads to a suppression. Regarding the loop-induced coupling to gluons, in the Type I model, C_g^h is equal to C_F^h (up to NLO), the dependence of which on $|c_{\beta-\alpha}|$ was presented in Fig. 4. In the case of Type II, C_g^h and C_U^h are very similar despite the difference between up- and down-type couplings, this being due to the fact that the b-loop contribution to C_g^h is rather small. The one exception in the case of Type II arises for the opposite-sign scenarios for which the b-loop contribution changes sign and interferes *constructively* with the t-loop contribution. For these latter cases, C_g^h is always enhanced, $C_g^h \sim 1.06$ [53].

While the exceedingly small deviations in C_V^h that we consider here will most likely not be directly accessible at the LHC, precision measurements of the other couplings together with a measurement of, or a limit on, $m_{H,A}$ can be used for consistency checks and for eventually pinning down the model. Of special interest in this context is also the triple Higgs coupling. The dependence of $C_{hhh} \equiv g_{hhh}/g_{hhh}^{\rm SM}$ on $c_{\beta-\alpha}$ and m_H is shown in Fig. 8. It is quite striking that large values of $C_{hhh} > 1$ (up to $C_{hhh} \approx 1.7$ in Type I and up to $C_{hhh} \approx 1.5$ in Type II) can be achieved in the nondecoupling regime, roughly $m_H \lesssim 600$ GeV, for $|c_{\beta-\alpha}|$ values of the order of 0.1, whereas for heavier m_H, C_{hhh} is always suppressed as compared to its SM prediction. These features were explained in the discussion below Eq. (67).[18] Note also that for $m_H \sim 1$ TeV C_{hhh} approaches the SM limit of 1 as $|c_{\beta-\alpha}|$ decreases more slowly than is the case for lighter m_H; substantial deviations $C_{hhh} < 1$ are possible as long as $|c_{\beta-\alpha}|$ is roughly greater than a few times 10^{-2}. This comes from the $(2Z_6/Z_1)c_{\beta-\alpha}$ term in Eq. (67): since, in the convention where $s_{\beta-\alpha} \geq 0$, $Z_6 c_{\beta-\alpha}$ is always negative, cf. Eq. (46), and since Z_6 can be sizable when $m_H \sim 1$ TeV, see Fig. 1, this can lead to a suppression as extreme as $C_{hhh} \approx 0.1$. (For $m_H \gg 1$ TeV, the deviations are smaller in part because the possible range of $c_{\beta-\alpha}$ is limited as seen in Fig. 1.) For very light m_H, on the other hand, Z_6 is much smaller, and hence the deviations with $C_{hhh} < 1$ are more limited. For

[18]This cannot be seen directly in Fig. 8, but we verified that points with $m_H > 630$ GeV never have $C_{hhh} > 1$.

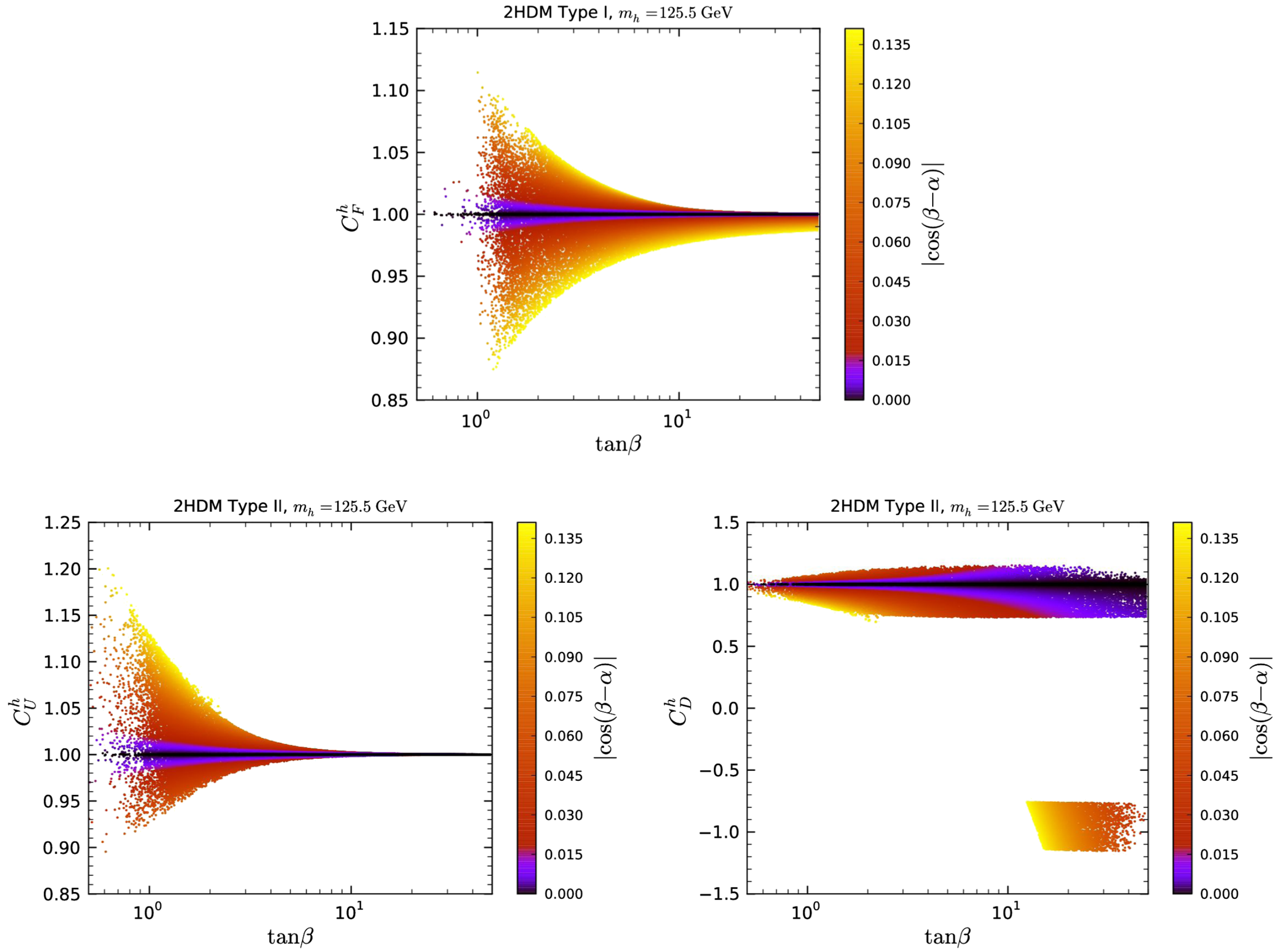

FIG. 6 (color online). Fermionic couplings vs $\tan\beta$ in Type I (upper panel) and Type II (lower panels) with the $|c_{\beta-\alpha}|$ color code. Points are ordered from high to low $|c_{\beta-\alpha}|$.

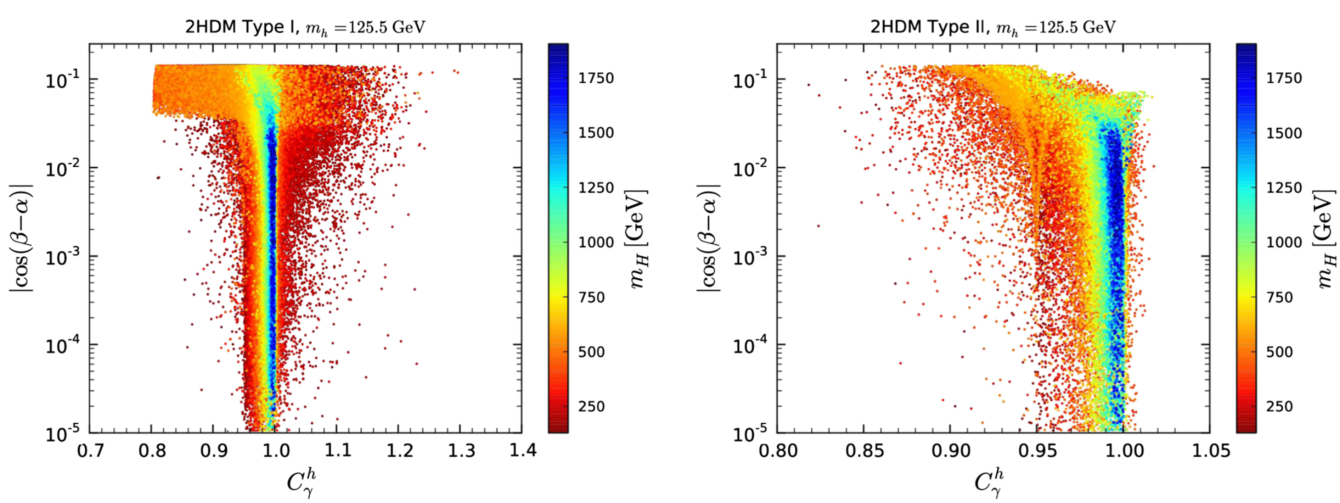

FIG. 7 (color online). $|c_{\beta-\alpha}|$ vs C_γ^h in Type I (left) and Type II (right) with the m_H color code. Points are ordered from low to high m_H.

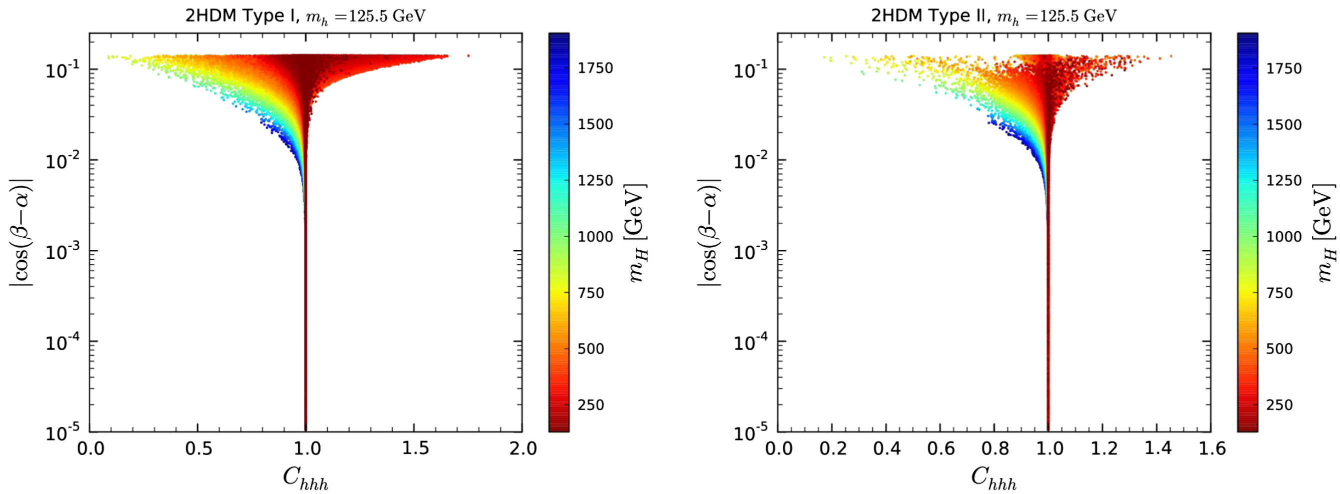

FIG. 8 (color online). $|c_{\beta-\alpha}|$ vs the reduced triple Higgs coupling C_{hhh} in Type I (left) and Type II (right) with the m_H color code. Points are ordered from high to low m_H values.

$m_H \lesssim 250$ GeV, we find $C_{hhh} \approx 0.80$–1.40 in Type I and $C_{hhh} \approx 0.90$–1.35 in Type II. This is at the limit of what can be measured, as the expected precision is about 50% at the high-luminosity options of the LHC and the ILC with 500 GeV and about 10%–20% at a 1–3 TeV e^+e^- linear collider with polarized beams [28].

The relation between the triple Higgs coupling g_{Hhh}, $|c_{\beta-\alpha}|$ and m_H is presented in Fig. 9. In Type I, large values of g_{Hhh} can be achieved in the nondecoupling regime for $|c_{\beta-\alpha}|$ of the order 10^{-1}. This is also true in Type II, though the range of g_{Hhh} is somewhat smaller. We observe moreover that for given $|c_{\beta-\alpha}| \lesssim 10^{-1}$ the achievable Hhh coupling grows with m_H. Nonetheless, as will be shown in Sec. IV D, the $H \to hh$ decay is mostly relevant below the $t\bar{t}$ threshold. Moreover, in the exact alignment limit, the Hhh coupling vanishes.

C. Signal strengths

The variations in the couplings to fermions discussed above have direct consequences for the signal strengths of the SM-like Higgs boson. Since the results depend a lot on the fermion coupling structure, we examine this separately for Type I and Type II.

Let us start with Type I. Figure 10 shows the signal strengths for gluon-gluon fusion and decay into $\gamma\gamma$ [$\mu^h_{gg}(\gamma\gamma)$, left panel] and decay into ZZ^* [$\mu^h_{gg}(ZZ^*)$, right panel]. Recalling that C^h_F varies between 0.87 and 1.11 in Type I and comparing with Fig. 7, it is clear that the variation in $\mu^h_{gg}(\gamma\gamma)$ comes to a large extent from the charged Higgs contribution to the $\gamma\gamma$ loop. Even for $|c_{\beta-\alpha}| \to 0$, large deviations from 1 can occur due to a sizable charged Higgs contribution or the presence of a light pseudoscalar $m_A < m_h/2$ that increases the SM-like Higgs total width. On the

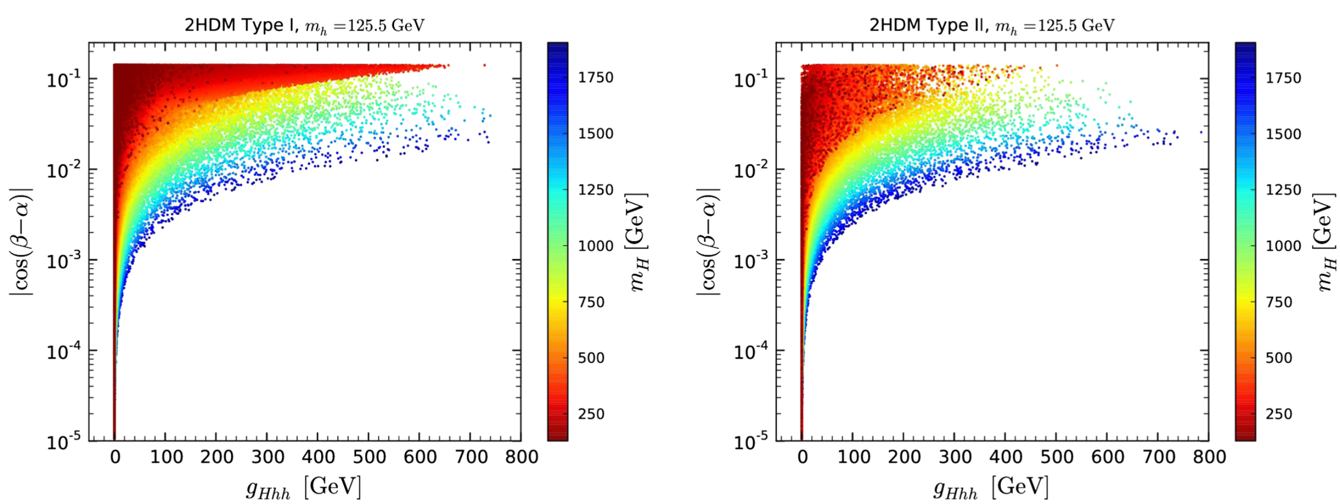

FIG. 9 (color online). $|c_{\beta-\alpha}|$ vs the triple Higgs coupling g_{Hhh} in Type I (left) and Type II (right) with the m_H color code. Points are ordered from high to low m_H values.

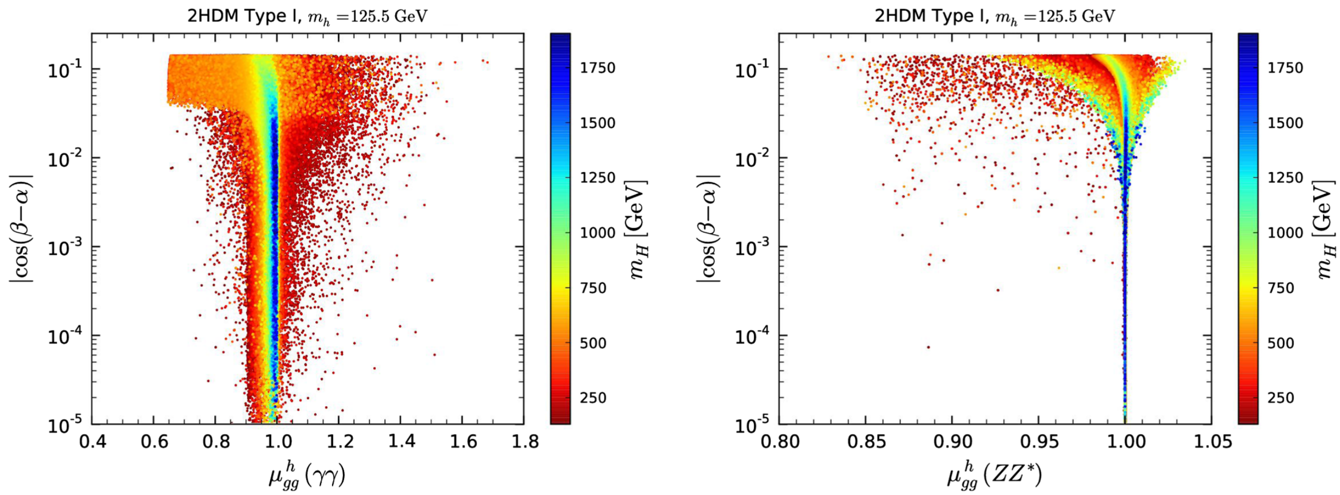

FIG. 10 (color online). Signal strengths in Type I for the 125.5 GeV state, for $gg \to h \to \gamma\gamma$ (left) and $gg \to h \to ZZ^*$ (right) with the m_H color code. Points are ordered from low to high m_H values. Points with $\mu^h_{gg}(ZZ^*) < 0.92$ are ones for which $h \to AA$ decays are present, so that the total h width is increased, which suppresses this particular channel's rate.

other hand, in the decoupling limit, the charged Higgs loop is small, and C^h_γ is largely determined by the relative size of the top and bottom loops compared to the W loop (which enters with opposite sign). On the contrary, C^h_g is solely determined by the size of the t- and b-loop contributions. One finds numerically that the $h\gamma\gamma$ coupling is more suppressed than the hgg coupling is enhanced, so that $\mu^h_{gg}(\gamma\gamma) \lesssim 1$ in the decoupling regime.

In contrast, $\mu^h_{gg}(ZZ^*)$ shows less variation, $\mu^h_{gg}(ZZ^*) = [0.92, 1.04]$, if the $h \to AA$ decay channel is closed, with small excursions around 1 allowed in the decoupling limit. It also exhibits a less distinct dependence on m_H compared to $\mu^h_{gg}(\gamma\gamma)$. The reason is that $\mu^h_{gg}(ZZ^*)$ is driven by C^h_F and $\tan\beta$, as illustrated in Fig. 11. The dependence on C^h_F is clear as larger (smaller) C^h_F leads to a larger (smaller) cross section for $gg \to h$. The dependence on $\tan\beta$ results from an interplay between the top (which drives the $gg \to h$ cross section) and bottom (which drives the total h width) Yukawa couplings both given by $C^h_F = s_{\beta-\alpha} + c_{\beta-\alpha}/t_\beta$. The scattered points with suppressed $\mu^h_{gg}(ZZ^*)$ are those where the $h \to AA$ decay mode is open and increases the total width. An analogous picture emerges for the VBF-induced $h\tau\tau$ signal strengths, since $\mu^h_{\rm VBF}(\tau\tau) = \mu^h_{gg}(ZZ^*)$ in Type I.

In Type II, we find that the situation is quite different. Here, the signal strengths are driven by both the top quark coupling, which impacts C^h_g, and by the bottom Yukawa coupling C^h_D, which also enters C^h_g and, often of greatest importance, determines the $h \to b\bar{b}$ decay width. In Fig. 12, we therefore show the signal strengths $\mu^h_{gg}(\gamma\gamma)$,

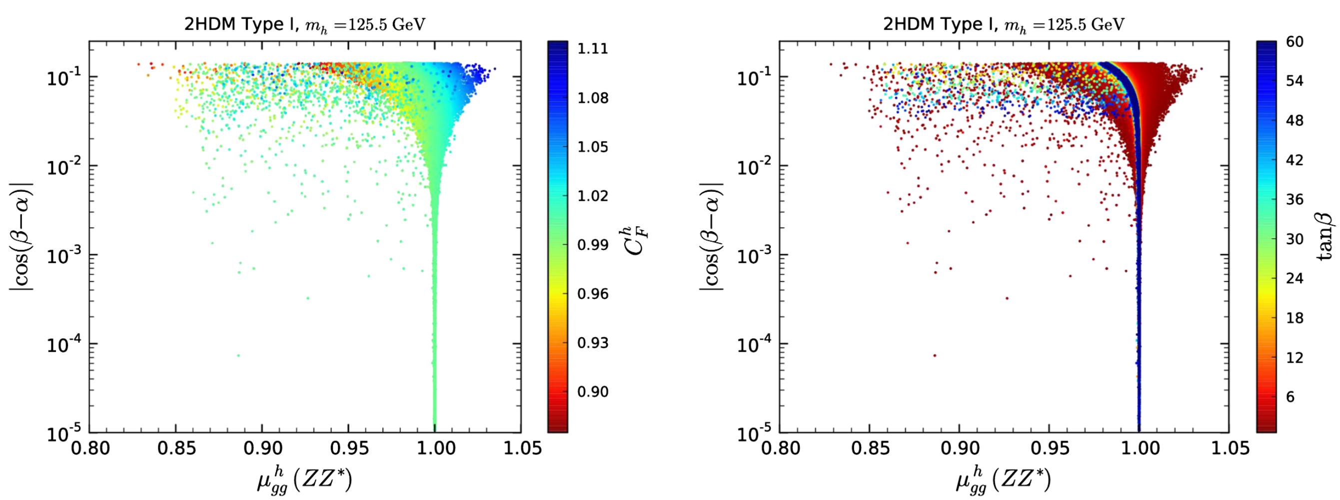

FIG. 11 (color online). Signal strength for $gg \to h \to ZZ^*$ in Type I for the 125.5 GeV state with the C^h_F (left) and $\tan\beta$ (right) color code. Points are ordered from low to high C^h_F and $\tan\beta$ values.

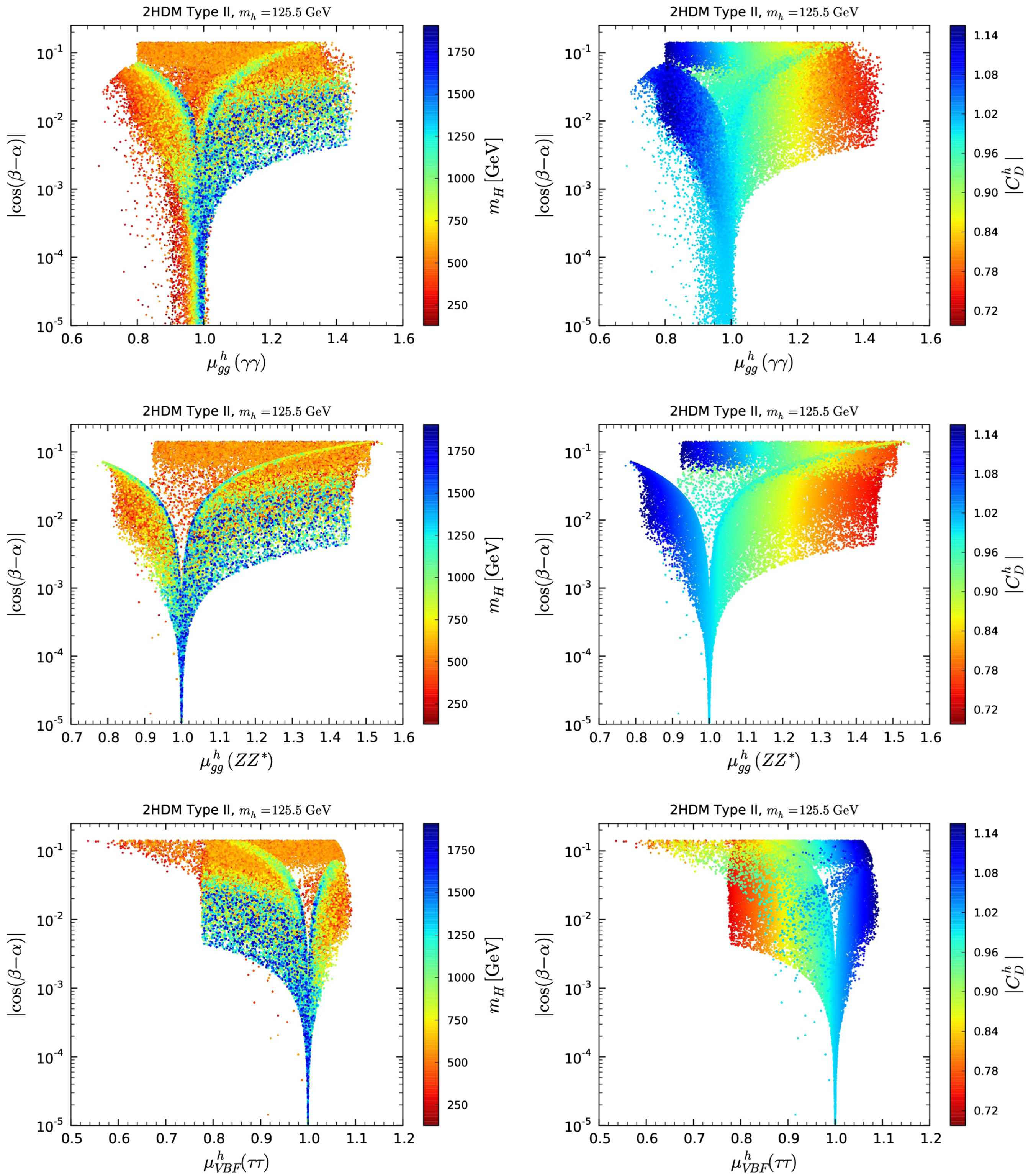

FIG. 12 (color online). Signal strengths in Type II for the 125.5 GeV state with the m_H (left) and $|C^h_D|$ color code. Points are ordered from low to high m_H and $|C^h_D|$ values.

$\mu^h_{gg}(ZZ^*)$, and $\mu^h_{\mathrm{VBF}}(\tau\tau)$ in Type II comparing the dependence on m_H (left panels) to the dependence on $|C^h_D|$ (right panels). Note that the m_H dependence of the signal strengths reflects the m_H dependence of C^h_D in Fig. 5. As a consequence, $\mu^h_{gg}(\gamma\gamma)$ and $\mu^h_{gg}(ZZ^*)$ can be enhanced in the decoupling regime, with values going as high as 1.4–1.5 (mainly due to the suppression of the total h width), to be compared to the current model-independent 95% C.L.

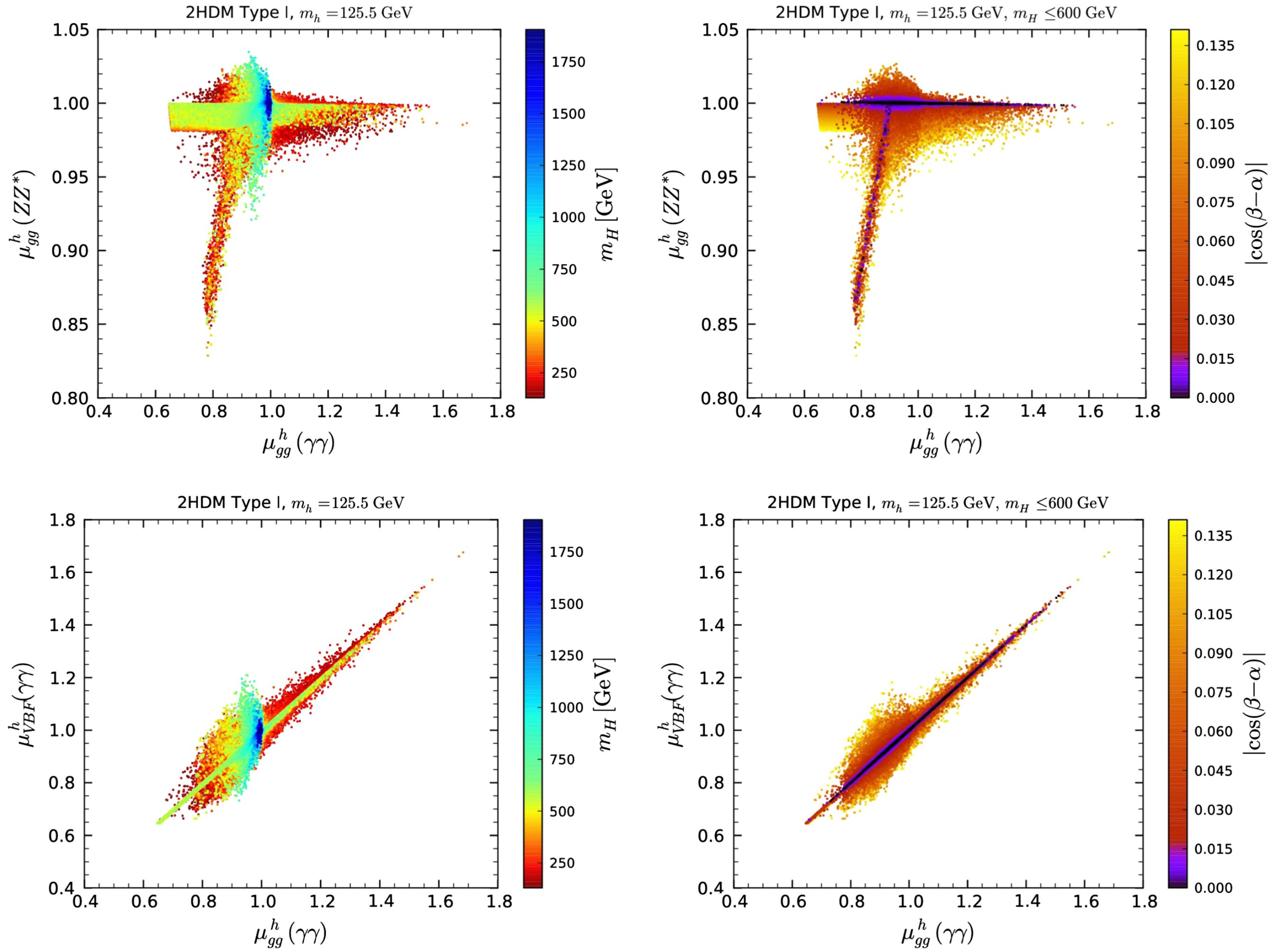

FIG. 13 (color online). Correlations of signal strengths in Type I, on the left illustrating the dependence on m_H and on the right illustrating the dependence in $|c_{\beta-\alpha}|$. Points are ordered from low to high m_H values (left) and high to low $|c_{\beta-\alpha}|$ values (right).

limits of $\mu^h_{gg}(\gamma\gamma) \in [0.76, 1.69]$ and $\mu^h_{gg}(ZZ^*) \in [0.71, 1.80]$. Suppression is also possible, reaching a level of 0.7 for low m_H if $|c_{\beta-\alpha}| > 0.01$ but limited to 0.9 for large $m_H \gtrsim 1250$ GeV. For all m_H, the amount of possible suppression decreases systematically with decreasing $|c_{\beta-\alpha}|$. For $\mu^h_{\rm VBF}(\tau\tau)$, the behavior is exactly the opposite. For completeness, we note that the horizontal bar at $|c_{\beta-\alpha}| \sim 10^{-1}$ is the $C^h_D < 0$ region, and the scattered points are those where the $h \to AA$ decay is open. Finally, note that as $|c_{\beta-\alpha}|$ decreases the signal strengths in Type II converge to 1 much more slowly than in Type I. This is a consequence of the delayed alignment of C^h_D to 1 in Type II when $\tan\beta$ is large. An additional effect arises in $\mu^h_{gg}(\gamma\gamma)$ due to the charged Higgs loop contribution to the $h \to \gamma\gamma$ amplitude. In particular, there exists an intermediate range of charged Higgs masses[19] for which $g_{hH^+H^-} \sim -2m^2_{H^\pm}/v$ [cf. Eq. (B8)], which yields a constant nondecoupling contribution that suppresses the $h \to \gamma\gamma$ amplitude [53] (see also Refs. [97,98]). Indeed, even for values of $|c_{\beta-\alpha}|$ as low as 10^{-4}, this signal strength does not converge to 1 until m_H (and thus $m_{H^\pm}$) is above about 1 TeV.

Putting everything together, we find quite distinct correlations of signal strengths in both Type I and Type II that depend on whether the additional Higgs states are decoupled or not. This is illustrated in Fig. 13 for Type I and in Fig. 14 for Type II. In both figures, the panels on the left show the dependence on m_H, while the panels on the right show the dependence on $|c_{\beta-\alpha}|$ for the nondecoupling regime with $m_H \leq 600$ GeV. We note that there are definite combinations of signal strengths that cannot be reached in the decoupling regime. A measurement of such values would be a very strong motivation to look for additional light Higgs states. In turn, when the masses of additional light Higgs states are measured, signal strength correlations as shown in Figs. 13 and 14 can help pin down the model. Furthermore, for $m_H \leq 600$ GeV, even in the apparent alignment limit

[19] In this intermediate mass region, the charged Higgs mass is given by Eq. (33), where $Y_2 \sim \mathcal{O}(v^2)$ and $Z_3 \gtrsim 1$ such that the upper bound of Z_3 is constrained by its unitarity bound.

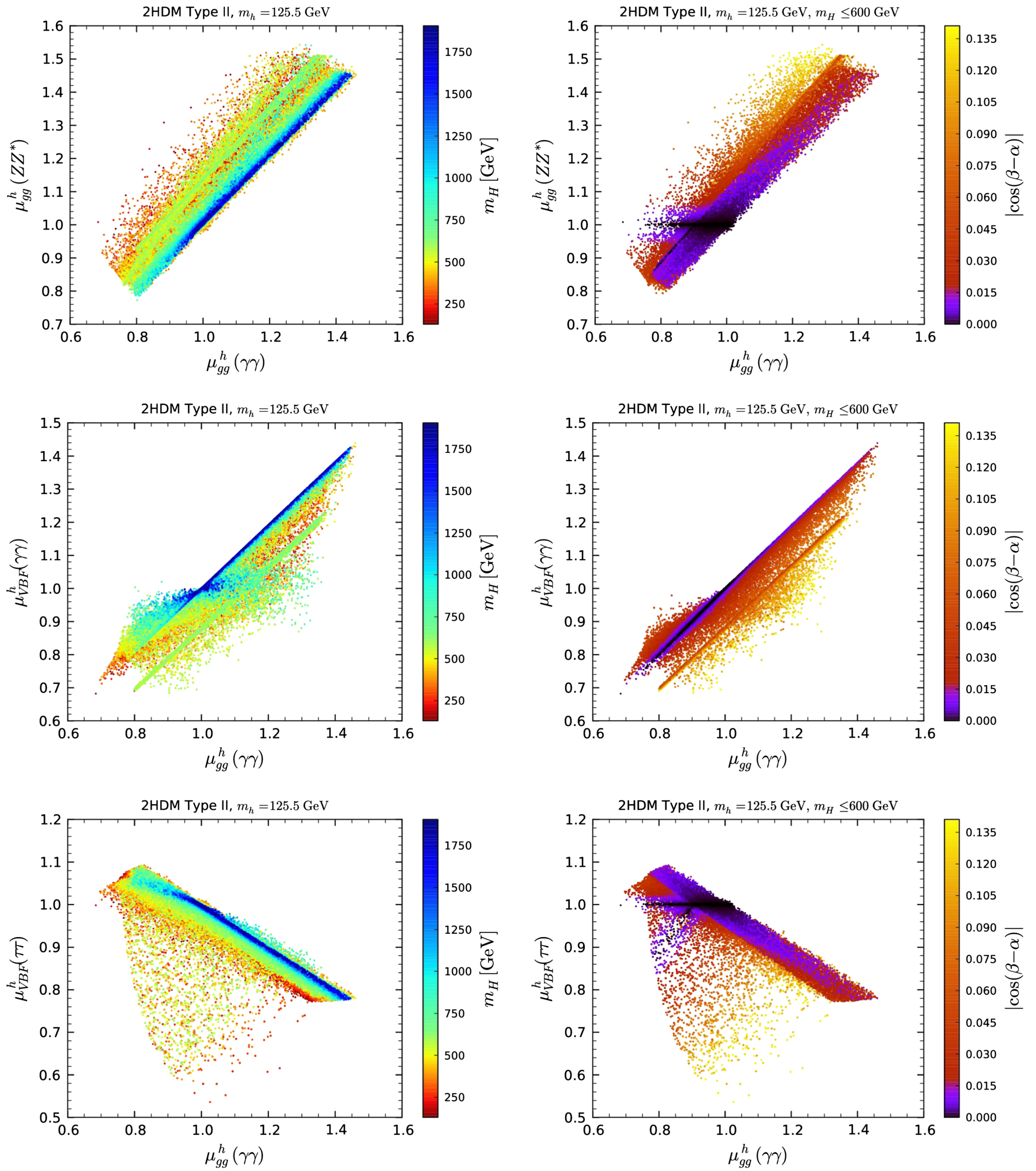

FIG. 14 (color online). Correlations of signal strengths in Type II, on the left illustrating the dependence on m_H, on the right illustrating the dependence in $|c_{\beta-\alpha}|$. Points are ordered from low to high m_H values (left) and high to low $|c_{\beta-\alpha}|$ values (right).

$|c_{\beta-\alpha}| \to 0$, there can be deviations in the signal strengths from unity that cannot be mimicked by decoupling.

Examples for Type I are the suppression of both $\mu^h_{gg}(\gamma\gamma)$ and $\mu^h_{gg}(ZZ^*)$, or the combination $\mu^h_{gg}(\gamma\gamma) > 1$ with $\mu^h_{gg}(ZZ^*) \approx 1$. The former case is also present in Type II for light m_H, while the latter does not occur at all in Type II. More concretely, in the decoupling regime of Type II, $\mu^h_{gg}(\gamma\gamma) \approx \mu^h_{gg}(ZZ^*)$, whereas for light m_H, one can have

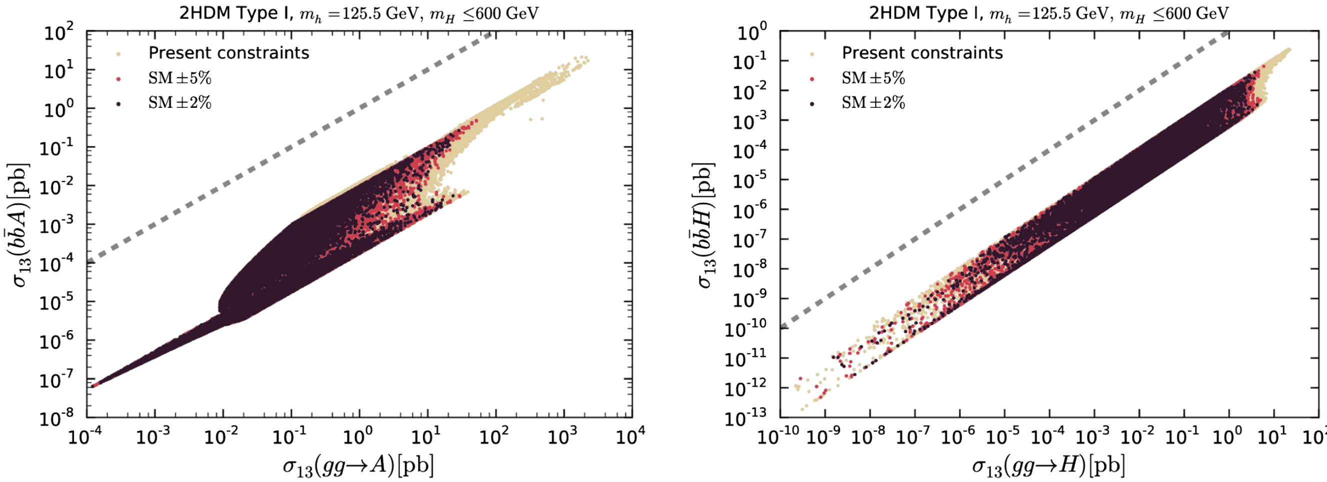

FIG. 15 (color online). $\sigma(b\bar{b}X)$ vs $\sigma(gg\to X)$ for $X=A$ (left) and $X=H$ (right) in Type I at the 13 TeV LHC for points satisfying all present constraints (in beige) as well as points for which the signals strengths from Eq. (80) are within 5% and 2% of the SM predictions (in red and dark red, respectively). The dashed lines indicate $\sigma(b\bar{b}X)=\sigma(gg\to X)$.

$\mu^h_{gg}(\gamma\gamma) < \mu^h_{gg}(ZZ^*)$ even if $|c_{\beta-\alpha}|$ is very small (comparing Fig. 14, top row, left vs right). Another example is the simultaneous suppression or enhancement of $\mu^h_{gg}(\gamma\gamma)$ and $\mu^h_{\rm VBF}(\gamma\gamma)$ in Type I, that is not possible in the decoupling regime (cf. Fig. 13, bottom left). In Type II, one can have a simultaneous enhancement, up to 1.45 of $\mu^h_{gg}(\gamma\gamma)$ and $\mu^h_{\rm VBF}(\gamma\gamma)$ in the decoupling regime, but simultaneous suppression is limited to ∼0.9–0.95 (cf. Fig. 14, middle left); simultaneous suppression to a level of ∼0.8 is, however, possible in the alignment limit for $m_H \lesssim 300$ GeV, i.e. well away from the decoupling regime. Precise enough signal strength measurements could therefore provide strong hints that we are in the alignment without the decoupling regime of a 2HDM even if no additional Higgs states are discovered at that time.

D. Cross sections for H and A production

Let us now turn to the prospects of discovering the additional neutral states. The two largest production modes at the LHC are gluon fusion, $gg\to X$, and the associated production with a pair of b-quarks, $b\bar{b}X$, with $X=A,H$. The correlations of the $gg\to X$ and $b\bar{b}X$ cross sections at the 13 TeV LHC in the nondecoupling regime $m_H \le 600$ GeV are shown in Fig. 15 for the Type I model and in Fig. 16 for the Type II model. We show the points that pass all present constraints (in beige) and highlight those that have a very SM-like 125 GeV Higgs state by constraining all the following signal strengths to be within 5% or 2% of their SM values, respectively, denoted as SM ± 5% (red) and SM ± 2% (dark red):

$$\mu^h_{gg}(\gamma\gamma),\quad \mu^h_{gg}(ZZ^*),\quad \mu^h_{gg}(\tau\tau),\quad \mu^h_{\rm VBF}(\gamma\gamma),$$
$$\mu^h_{\rm VBF}(ZZ^*),\quad \mu^h_{\rm VBF}(\tau\tau),\quad \mu^h_{VH}(b\bar{b}),\quad \mu^h_{t\bar{t}}(b\bar{b}). \qquad (80)$$

We start the discussion with the production of A in Type I, shown in the left panel of Fig. 15. There is a strong correlation between the two production modes, gluon fusion and $b\bar{b}$ associated production, which stems from the fact that the relevant couplings are the same up to a sign: $C^A_U = -C^A_D = \cot\beta$. The larger spread in $\sigma(b\bar{b}A)$ observed for $\sigma(gg\to A) > 10^{-2}$ pb comes from the fact that for $m_A \lesssim 400$ GeV the $b\bar{b}A$ cross section grows faster with decreasing m_A than that of $gg\to A$. Therefore, along a line of fixed $\sigma(gg\to A)$ in the plot, a point with higher $\sigma(b\bar{b}A)$ has a smaller m_A. Note also that there is an interference of the top- and bottom-loop diagrams in $gg\to A$ which changes sign depending on m_A. Overall, however, $\sigma(gg\to A)$ is always at least 2 orders of magnitude larger than $\sigma(b\bar{b}A)$.

The points with the largest cross sections, $\sigma(b\bar{b}A)\approx 10$ pb and $\sigma(gg\to A)\approx 1000$ pb, correspond to the case $m_A < m_h/2$ which was studied in detail in Ref. [27]. One feature of this region is that $\mu^h_{gg}(\gamma\gamma)$ and $\mu^h_{gg}(ZZ^*, WW^*)$ always differ from each other by about 10%. Constraining all h signal strengths of Eq. (80) within 5% of unity therefore eliminates these points. Other points with high cross sections, but not in the very light pseudoscalar region, would also be eliminated by the SM ± 5% or SM ± 2% requirement. However, in this nondecoupling regime of $m_H \le 600$ GeV, points with sizeable cross sections up to 0.2 pb for $\sigma(b\bar{b}A)$ and up to about 40 pb for $\sigma(gg\to A)$ still remain even at the SM ± 2% level. At this same SM ± 2% level, the smallest $\sigma(gg\to A)$ is about 0.1 fb.

Regarding production of the scalar H in Type I, shown in the right panel of Fig. 15, the correlation is even stronger between $\sigma(b\bar{b}H)$ and $\sigma(gg\to H)$ since both are driven by the same fermionic coupling $C^H_F = \sin\alpha/\sin\beta$. Note that, as in the A case, the gluon-fusion cross section is always

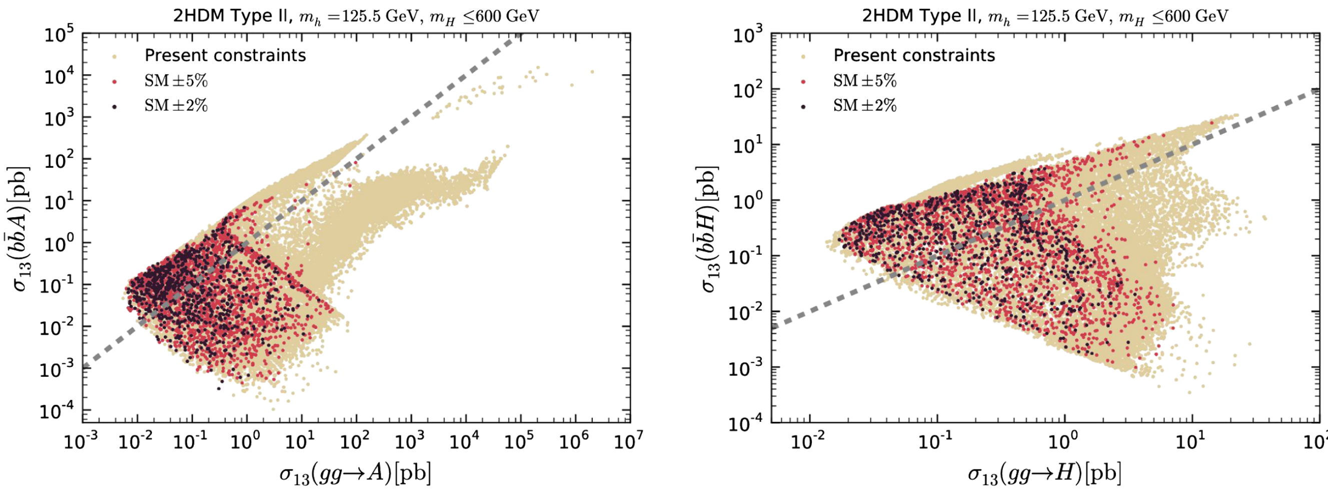

FIG. 16 (color online). As in Fig. 15 but for Type II.

larger than that for $b\bar{b}$ associated production. Sizable cross sections are still allowed under the SM $\pm$ 2% constraint, which implies that in the nondecoupling regime there is a strong possibility of detecting a non-SM-like scalar state at the LHC. The structure of C_F^H is, however, such that the coupling can equally well be very much suppressed, leading to extremely small cross sections. We will come back to this below.

The corresponding results for Type II are presented in Fig. 16. In contrast to Type I, both $b\bar{b}$ associated production and gluon–gluon fusion modes for Type II are in principle important since either can be dominant in different regions of the parameter space. There is only modest correlation between the two production modes due to the more complex structure of the Type II fermionic couplings. For A production, one clearly sees the $m_A < m_h/2$ region as the detached scattered points with very large cross sections. As for Type I, these points disappear under the SM $\pm$ 5% constraint. Still, even for SM $\pm$ 2%, cross sections as large as $\sigma(b\bar{b}A) \approx 8$ pb and $\sigma(gg\to A) \approx 20$ pb can be achieved (although not simultaneously). For H production, a similar picture emerges, with the cross sections, however, being a factor of a few smaller than for A production. The minimal cross sections in this $m_H <$ 600 GeV nondecoupling regime for the A and H are correlated in a way that is very favorable for discovery during Run 2 of the LHC. For example, if $\sigma(gg \to A)$ takes on its minimum SM $\pm$ 2% value of 10 fb, then $\sigma(b\bar{b}A) \gtrsim 80$ fb, whereas if $\sigma(b\bar{b}A)$ takes on its minimal value of few $\times\, 10^{-1}$ fb, then $\sigma(gg \to A) \approx 10^3$ fb. These cross section levels imply that the A should be discoverable in at least one of the two production modes even in the extreme alignment limit.

Before considering specific decay channels of A and H, we present in Fig. 17 the gluon-fusion cross sections in Type I and Type II as functions of m_A and m_H at the 13 TeV LHC. Here, the color code shows the dependence on $\tan\beta$.[20] In Type I, the $gg \to A$ cross section is proportional to $\cot^2\beta$; this explains why it is larger (smaller) at lower (higher) $\tan\beta$. A cross section of 1 (0.1) fb is guaranteed for m_A as large as ∼600(850) GeV. On the other hand, the $gg \to H$ cross section in Type I is proportional to $(C_F^H)^2$ and can take on extremely small values for $m_H \lesssim 850$ GeV. The reason is that, in this region, the reachable values of $c_{\beta-\alpha}$ are high enough such that a cancellation between the two terms of $C_F^H = (s_{\beta-\alpha} - c_{\beta-\alpha}/t_\beta)$ occurs and leads to an almost vanishing coupling. In contrast, for $m_H \gtrsim 850$ GeV, this cancellation is not possible as the values of $c_{\beta-\alpha}$ are forced to be smaller as can be seen in Fig. 1. In Type II, the A production cross section can be very large in the very low m_A region as noted in Ref. [27], and any mass smaller than 1.1 (1.2) TeV gives a $gg \to A$ cross section larger than 1 (0.1) fb. For $gg \to H$, a cross section > 1 (0.1) fb is guaranteed up to $m_H \approx 850$ GeV (1.2 TeV). From these considerations, the prospects for discovering the additional neutral states look promising should alignment without decoupling be realized.

Let us now turn to specific signatures. Figure 18 presents the cross sections for $gg \to A \to Y$ for $Y = \gamma\gamma, \tau\tau, t\bar{t}$ in Types I and II. Note that the y-axis is cut off at 10^{-7} pb. Although much lower values of the cross section are possible, we do not show these lower values since they will certainly not be observable at the LHC. As expected, for the $\gamma\gamma$ and $\tau\tau$ final states, the cross sections fall sharply above the $t\bar{t}$ threshold, with the noticeable exception of the $A \to \tau\tau$ decay in Type II due to the strong constraints from LHC direct searches that exclude points with a large corresponding cross section. For the $A \to \gamma\gamma$ decay, cross sections of 0.1 fb are reachable for $m_A \lesssim 470$ GeV ($m_A \lesssim 530$ GeV) in Type I (II) but not guaranteed. The

[20]To avoid a proliferation of plots, we choose to show here only the results for gluon fusion; all corresponding results for the $b\bar{b}$ cross section can be provided upon request.

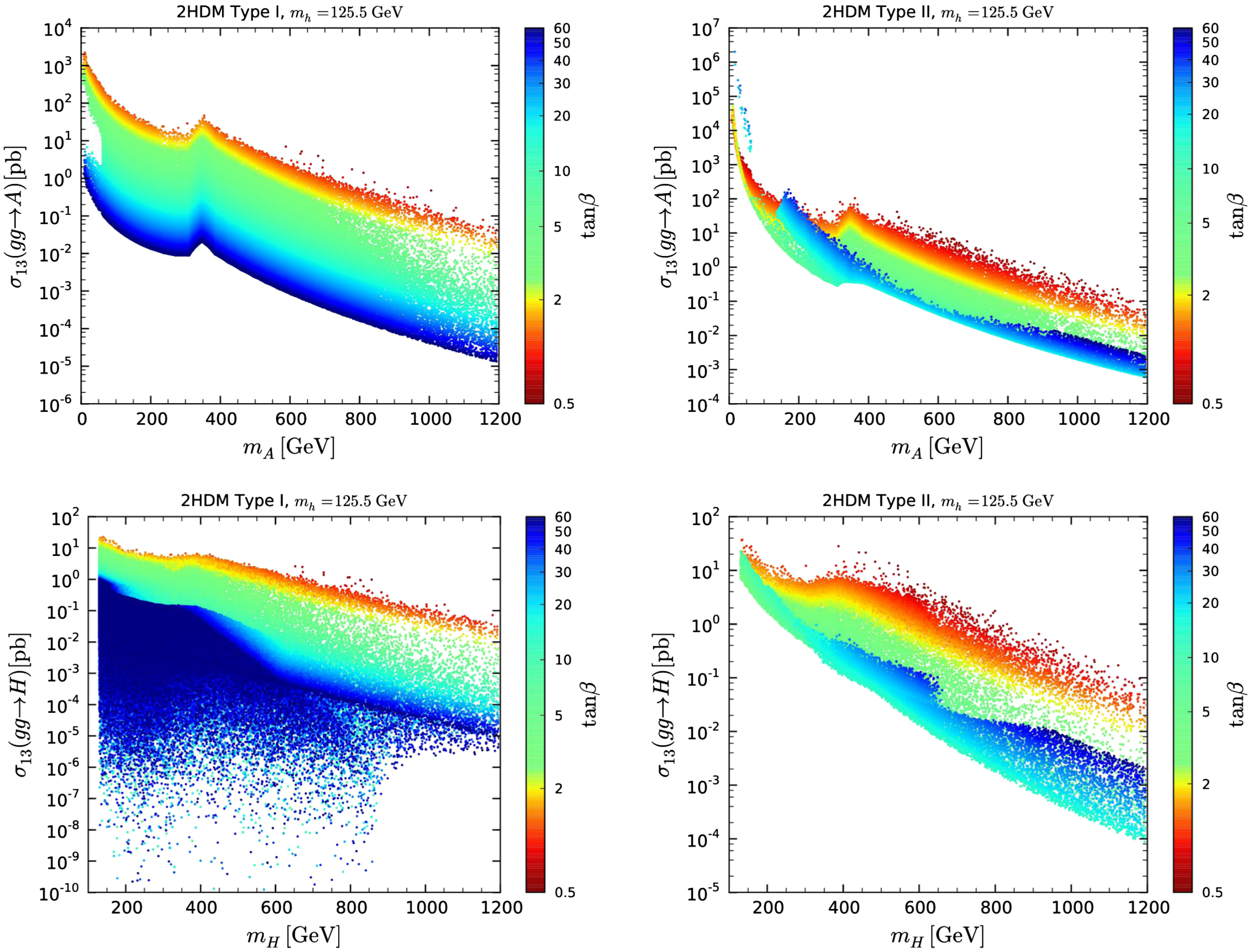

FIG. 17 (color online). Cross sections in Type I (left) and Type II (right) for $gg \to X$ at the 13 TeV LHC as functions of m_X for $X = A$ (upper row) and $X = H$ (lower row) with the $\tan\beta$ color code. In all four plots, points are ordered from low to high $\tan\beta$.

maximal cross section is ~30 fb in Type I and ~100 fb in Type II (not considering the $m_A \leq m_h/2$ region). In both Types I and II, the $gg \to A \to \tau\tau$ cross section can be substantially larger. In Type I, 0.1 fb is reachable for $m_A \lesssim 600$ GeV, while in Type II $m_A \lesssim 550$ GeV *guarantees* a cross section larger than 0.1 fb. In both cases, very large cross sections are predicted at low m_A. The $gg \to A \to t\bar{t}$ cross section peaks around 100 pb in both Types I and II and is guaranteed to be larger than 0.1 fb in Type II for $350 \lesssim m_A \lesssim 600$ GeV. These sizable cross sections therefore provide interesting probes of the extended Higgs sector in the alignment limit.

The corresponding results for the H cross sections are presented in Fig. 19. Sizable values of $\sigma\times$BR are possible in both Types I and II, but heavily suppressed values are still possible for most of the cases. Only in Type II, for $H \to \tau\tau$ (as well as for $H \to t\bar{t}$), is the corresponding cross section guaranteed to be larger than 0.1 fb for $m_H \lesssim 460$ GeV ($m_A \approx 400$ GeV). Note that, for both Types I and II, the cross sections for A/H decays into a muon pair are related to the $A/H \to \tau\tau$ ones through $\mathcal{B}(A/H \to \mu\mu) \approx (m_\mu/m_\tau)^2 \times \mathcal{B}(A/H \to \tau\tau) \approx \mathcal{B}(A/H \to \tau\tau)/280$.

Nonstandard production modes of the SM-like state, through $A \to Zh$ and $H \to hh$, are presented in Fig. 20. While these can be interesting discovery modes for the A and/or H, their cross sections can also be extremely suppressed. For $gg \to A \to Zh$, the $\tan\beta$ dependence, which follows the dependence of the $gg \to A$ cross section shown in Fig. 17, explains a part of this suppression. Moreover, the AZh coupling is proportional to $c^2_{\beta-\alpha}$ which is suppressed in the alignment region. Nevertheless, the $gg \to A \to Zh$ cross section can be of the order of 1 pb for $200 \lesssim m_A \lesssim 350$ GeV in both Types I and II. The $gg \to H \to hh$ cross section, as expected, attains its maximum below the $t\bar{t}$ threshold in both Types I and II and can reach about 10 pb at low $\tan\beta$. For any m_H, the cross section can, however, also be extremely suppressed.

A comment is in order here on the possible "feed down" (FD) [13,99] to the production of the 125 GeV state through the decay of heavier Higgs states, which might

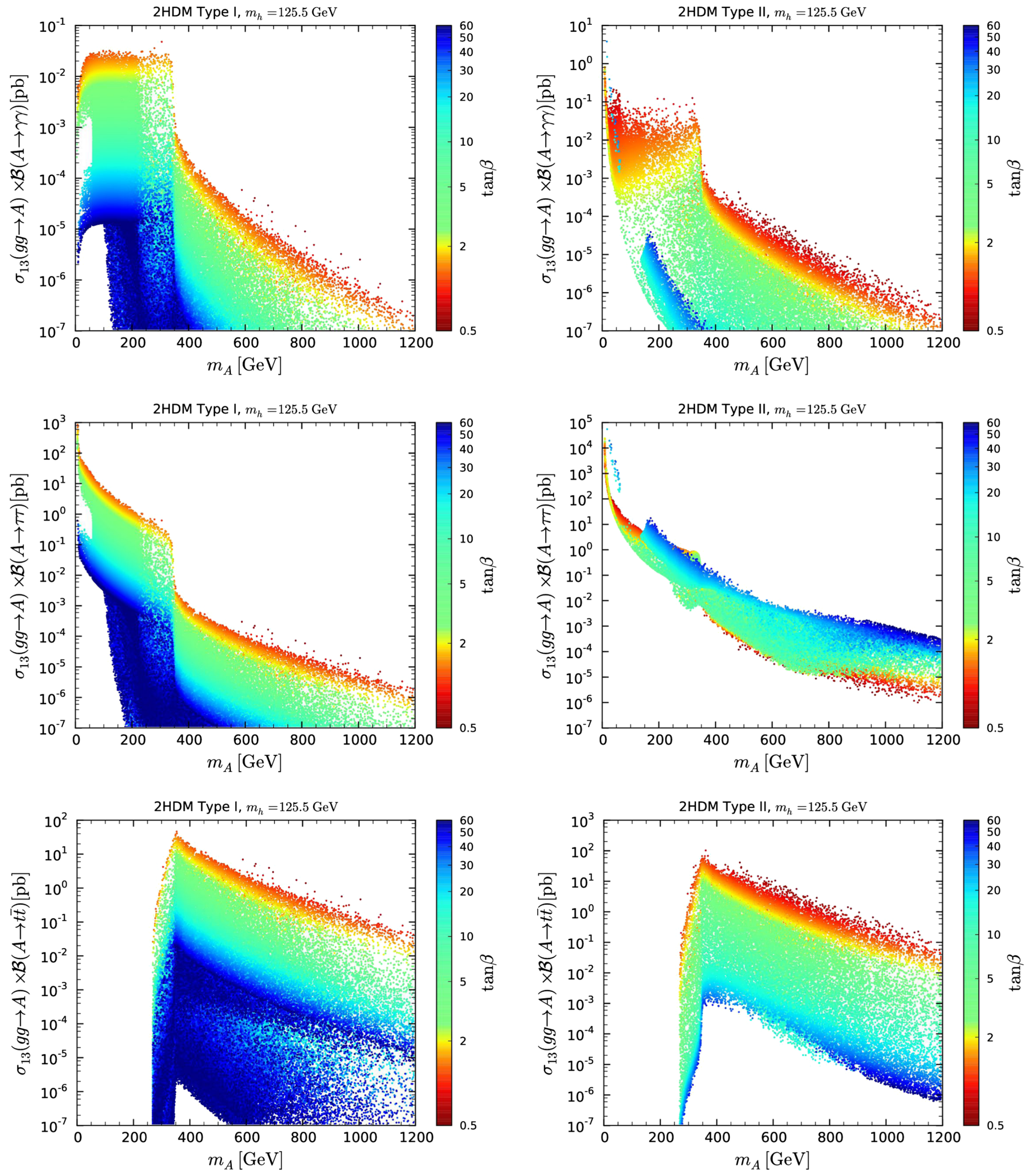

FIG. 18 (color online). Cross sections times branching ratio in Type I (left) and in Type II (right) for $gg \to A \to Y$ at the 13 TeV LHC as functions of m_A for $Y = \gamma\gamma$ (upper panels), $Y = \tau\tau$ (middle panels), and $Y = t\bar{t}$ (lower panels) with the $\tan\beta$ color code. Points are ordered from low to high $\tan\beta$.

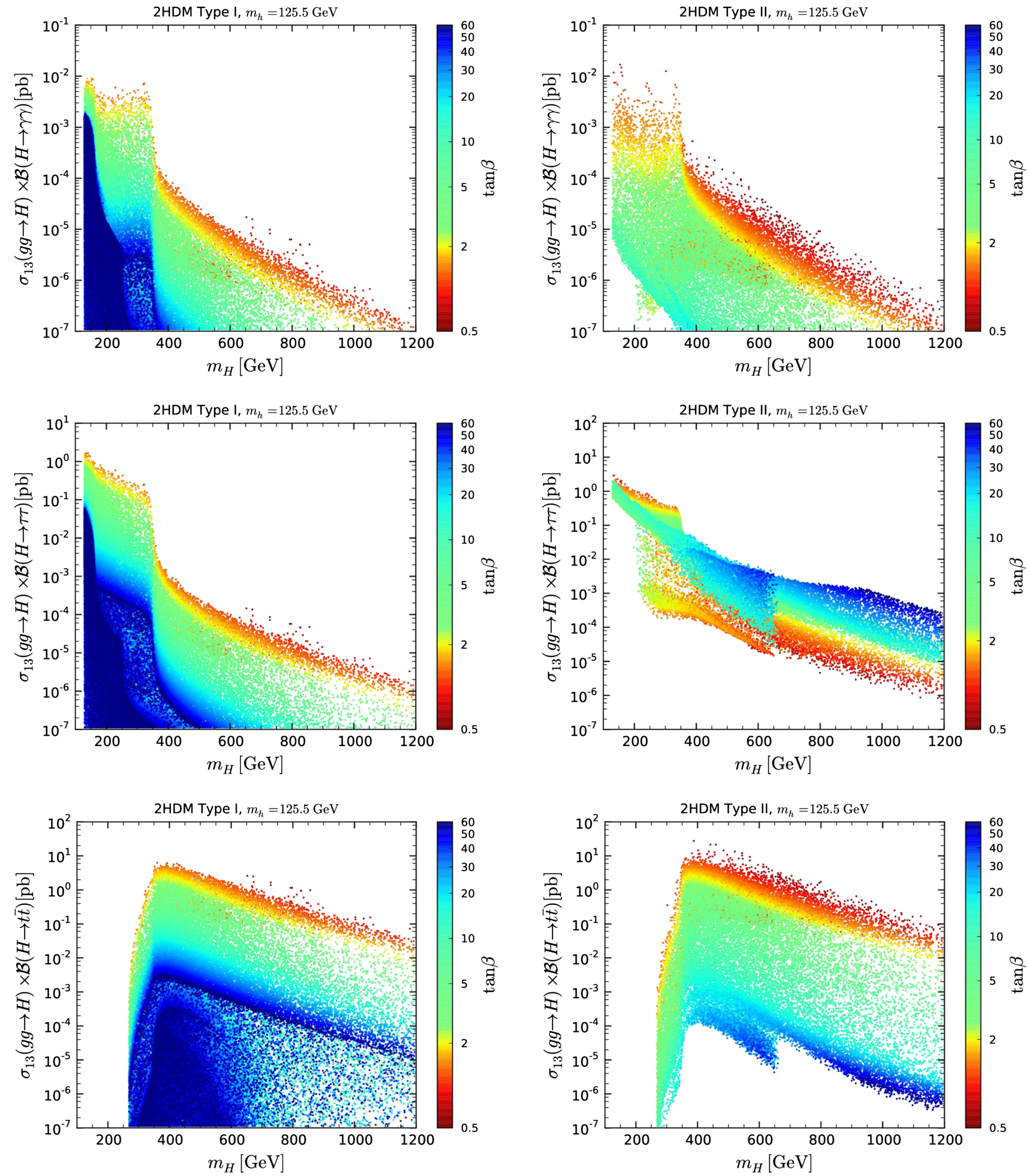

FIG. 19 (color online). Cross section times branching ratio in Type I (left) and in Type II (right) for $gg \to H \to Y$ at the 13 TeV LHC as functions of m_H for $Y = \gamma\gamma$ (upper panels), $Y = \tau\tau$ (middle panels), and $Y = t\bar{t}$ (lower panels) with $\tan\beta$ color code. Points are ordered from low to high $\tan\beta$.

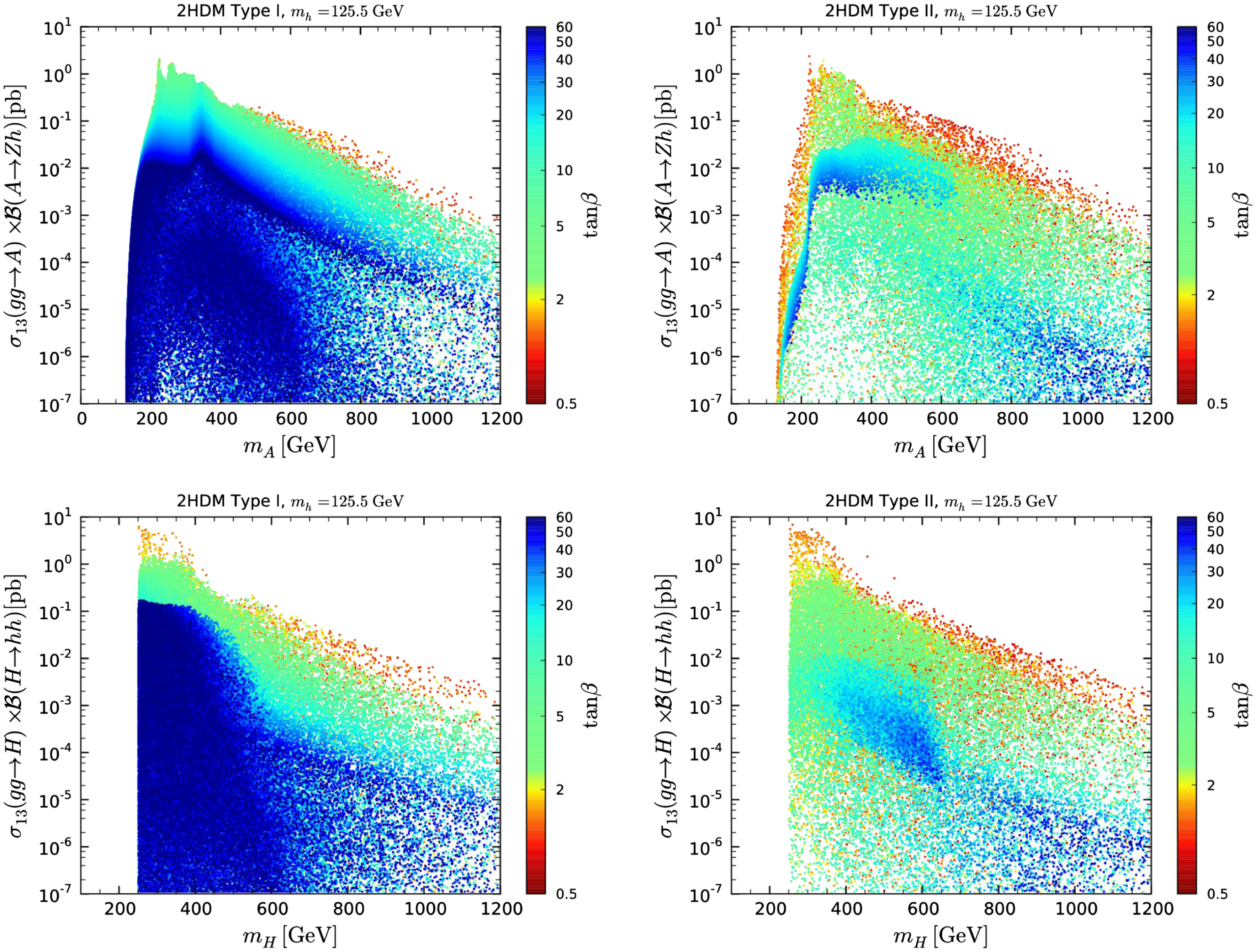

FIG. 20 (color online). Cross sections times branching ratio in Type I (left) and in Type II (right) for $gg \to X \to Y$ at the 13 TeV LHC as functions of m_X for $X, Y = A, Zh$ (upper panel) and $X, Y = H, hh$ (lower panel) with $\tan\beta$ color code. Points are ordered from low to high $\tan\beta$.

distort the Higgs signal strengths. This issue was approximately addressed in Sec. III.C of Ref. [13] by imposing the "FDOK" conditions $\mu^{\rm FD}_{Zh} < 0.3$ and $\mu^{\rm FD}_{{\rm ggF}h+bbh} < 0.1$, which limit the FD contamination of Zh associated production and of ggF + bbh production to 30% and to 10%, respectively, at the cross section times the branching ratio level. Imposing these conditions here would remove the points with $\sigma_{13}(gg \to A) \times {\rm BR}(A \to Zh) \gtrsim 0.2$ pb and $\sigma_{13}(gg \to H) \times {\rm BR}(H \to hh) \gtrsim 2$ pb in Fig. 20. This is, however, a maximally conservative constraint for two reasons. First, the amount of FD is computed without accounting for any reduced acceptance of such events into the 125 GeV signal as a result of the experimental cuts used to define the $gg \to h$, bbh, or $Z^* \to Zh$ channel. Second, it puts individual limits on specific production × decay modes instead of including all signal strengths in a global fit, which is the approach followed in this paper. Indeed, when directly adding the contribution of $gg \to A \to Zh$ to the Zh signal strength in the global fit, it turns out that only cross sections of $\sigma_{13}(gg \to A) \times {\rm BR}(A \to Zh) \gtrsim 1.6$ pb are definitely excluded. This still assumes that the signal acceptance of the experimental analysis is the same for $gg \to A \to Zh$ as for $gg \to Z^* \to Zh$, which should, however, be a reasonable approximation, as the main difference would be the Zh invariant-mass distribution, which is not used as a selection criterion in this case. The contribution of $H \to hh$ to the h signal strengths is a more difficult question, as here the acceptances (in each final state considered in the experimental analyses) will certainly be different from those of single h production. A detailed study based on event simulation would be necessary to better understand the impact of FD on the 125 GeV Higgs signal, but this is beyond the scope of this paper.

Finally, if the mass splitting is large enough, $A \to ZH$, $H \to ZA$, and $H \to AA$ decays offer intriguing possibilities for discovering the extra non-SM-like neutral Higgs states in the regime of approximate alignment without decoupling. In Fig. 21, the cross sections for $gg \to A \to ZH$,

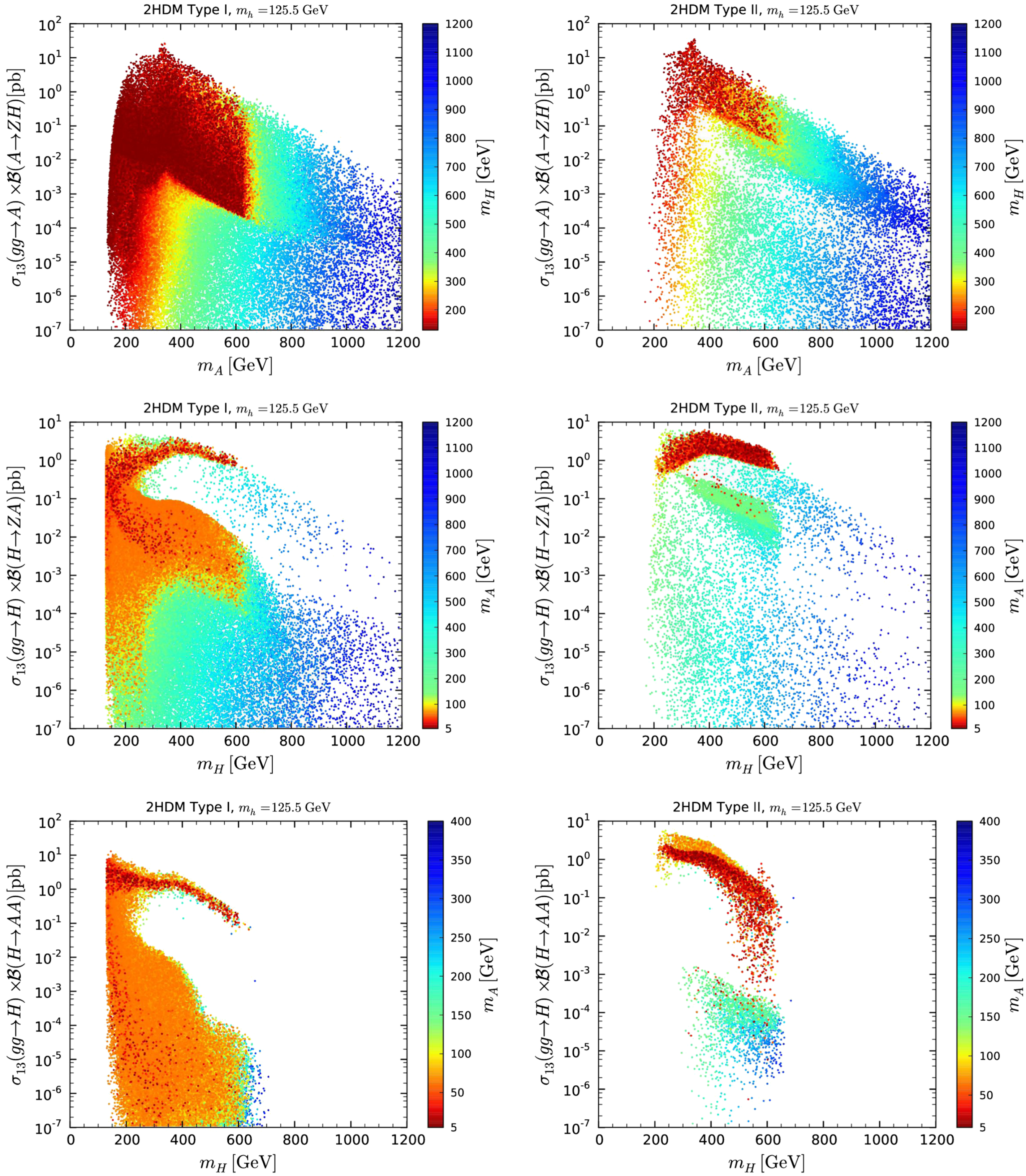

FIG. 21 (color online). Cross sections times branching ratio in Type I (left) and in Type II (right) for Higgs-to-Higgs signatures at the 13 TeV LHC, in the upper panel $gg \to A \to ZH$ with the m_H color code and in the middle and lower panels for $gg \to H \to ZA$ and $gg \to H \to AA$, respectively, with the m_A color code. Points are ordered from high to low m_A or m_H.

$gg \to H \to ZA$, and $gg \to H \to AA$ are exhibited. Large $gg \to A \to ZH$ cross sections are obtained for large $m_A - m_H$ splitting.[21] Looking back at Fig. 2, one sees that, in both Type I and Type II, the splitting can only be large for $m_A \lesssim 650$ GeV. This explains the preponderance of low m_H points with cross sections up to 20 pb for $m_A \lesssim 650$ GeV. However, $gg \to A \to ZH$ can also be heavily suppressed; since the AHZ coupling is proportional to $s_{\beta-\alpha}$, this suppression is a purely kinematical effect.

Turning to the $H \to ZA$ and $H \to AA$ signatures, we observe a depleted area for $m_H > 300$ GeV and cross sections of the order of 0.1 pb. In this region, $\tan\beta = 2$–10, and Z_5 is small or negative leading to m_H, m_A masses for which the $H \to ZA$, AA decays are kinematically forbidden [cf. Eq. (45)]. In the region below, $\tan\beta > 10$ and Z_5 can be large enough to achieve $m_H > m_A + m_Z$ and/or $m_H > 2m_A$, but nevertheless the cross section is small because of the $\tan\beta$ dependence of $\sigma(gg \to H)$; see Fig. 17. The distinct branch with $gg \to H \to ZA$ and $gg \to H \to AA$ cross sections larger than about 1 pb, on the other hand, has $\tan\beta \lesssim 2$ and $\lambda_5 \approx 0$. Here, the term proportional to $\sin 2\beta$ in Eq. (23) gives a large enough $Z_5 > 0$ so that the $H \to ZA$ and/or $H \to AA$ decay is kinematically allowed. The small $\tan\beta$ leads to a large $gg \to H$ production cross section; see again Fig. 17. The CMS Collaboration has very recently published a search for $A \to ZH$ and $H \to ZA$ [78]. For instance, for m_A (m_H) of about 200–600 GeV and very light H (A) below 100 GeV, the 95% C.L. limit on the relevant cross section is of the order of 30–50 fb in the $\ell\ell\tau\tau$ final state and 20–100 fb in the $\ell\ell b\bar{b}$ final state. Considering the branching ratios for $Z \to \ell\ell$ and $H \to \tau\tau, b\bar{b}$ $(A \to \tau\tau, b\bar{b})$, these limits just start to touch the highest cross sections in Fig. 21. A detailed phenomenological analysis of the $A \to ZH$ and $H \to ZA$ decays at the LHC was performed in Ref. [101].

Last but not least, note that, due to the kinematic constraint $m_H \geq 2m_A$ and the nontrivial correlation between m_H and m_A observed in Fig. 2, the $H \to AA$ channel is only open for $m_H \lesssim 700$ GeV. In Type I, the branch of points with cross sections ranging from about 10^{-1} to 10 pb is mainly populated by $m_A \leq 100$ GeV points with relatively low $\tan\beta \lesssim 10$. In Type II, points with low $m_A \lesssim 250$ GeV and $\tan\beta \lesssim 3$ are clearly separated from points with $m_A \gtrsim 150$ GeV and larger $\tan\beta \gtrsim 12$. This channel thus offers a complementary probe to the low m_A region discussed in Ref. [27].

V. CONCLUSIONS

While the Higgs measurements at Run 1 show no deviations from the SM, conceptually there is no reason why the Higgs sector should be minimal. Indeed a nonminimal Higgs sector is theoretically very attractive and, if confirmed, would shine a new light on the mechanism of electroweak symmetry breaking dynamics.

In this paper, we focused on CP-conserving 2HDMs of Type I and Type II, investigating the special situation that arises when one of the Higgs mass eigenstates is approximately aligned with the direction of the scalar field vacuum expectation values. In this case, the $W^\pm$ and Z gauge bosons dominantly acquire their masses from only one Higgs doublet of the Higgs basis. Moreover, the coupling of that CP-even Higgs boson to the gauge bosons tends toward the SM value, $C_V \to 1$. While this is automatically the case in the decoupling limit when the extra non-SM Higgs states are very heavy, such an alignment can also occur when the extra Higgs states are light, below about 600 GeV. We specifically investigated the phenomenological consequences of alignment without decoupling and contrasted them to the decoupling case. Two aspects are interesting in this respect: one being precision measurements of the couplings and signal strengths of the SM-like Higgs boson at 125 GeV and the other being the ways to discover the additional Higgs states of the 2HDM when they are light.

In addition to an in-depth theoretical discussion, we performed a detailed numerical analysis for the case that the SM-like state observed at 125 GeV is the lighter of the two CP-even Higgs bosons of the 2HDM, h. In this study, we allowed for 1% deviation from unity in C_V^h, which corresponds to the ultimate expected LHC precision at high luminosity. The results can be summarized as follows:

(1) In the alignment limit without decoupling, despite C_V^h being very close to 1, the fermionic couplings of the 125 GeV Higgs can deviate substantially from the SM values. Concretely, C_U^h can deviate as much as about 10% (20%) from unity in Type I (Type II) and C_D^h as much as 30% in Type II.

(2) While C_U^h rather quickly approaches 1 with increasing m_H and/or $c_{\beta-\alpha} \to 0$, the approach of the bottom Yukawa coupling to its SM value in the alignment limit is delayed in Type II, with $C_D^h \approx 0.70$–1.15 even for $|c_{\beta-\alpha}| \sim 10^{-2}$. Large values of $C_D^h > 1$ are associated with light H, A. Moreover, for 230 GeV $\lesssim m_H \lesssim 665$ GeV and $m_A \lesssim 650$ GeV, there is an allowed region with $C_D^h \approx -1 \pm 0.2$; this "opposite-sign" solution can be tested decisively at Run 2.

(3) The trilinear hhh coupling can also exhibit large deviations. Large values of $C_{hhh} > 1$ (up to $C_{hhh} \approx 1.7$ in Type I and up to $C_{hhh} \approx 1.5$ in Type II) can be achieved in the nondecoupling regime $m_H \lesssim 600$ GeV, for $|c_{\beta-\alpha}|$ of the order of 0.1, whereas for heavier m_H, C_{hhh} is always suppressed as compared to its SM prediction. The suppression can be about 50% for m_H of $\sim$1 TeV and much larger for lighter m_H.

[21] A large splitting $m_A - m_H \approx v$ can be motivated by the possibility of a strong first-order phase transition in 2HDMs [100].

(4) For the ratios $\mu_X^h(Y)$ of the $X \to h \to Y$ signal rates relative to the SM prediction, we found distinct correlations of these signal strengths in both Type I and Type II that depend on whether the additional Higgs states are decoupled or not. In fact, in the regime of alignment without decoupling, there are characteristic combinations of the $\mu_X^h(Y)$ signal strengths that cannot be mimicked by the decoupling limit. However, it is of course also possible that all signal strengths converge to 1 even though the additional Higgs states are very light.

(5) A decisive test of the alignment without decoupling scenario would of course be the observation of the additional Higgs states of the 2HDM in the mass range below about 600 GeV. We delineated the many possibilities for such observations. While there are no guarantees in the case of the Type I model, in the Type II model, there is always a definite lower bound on the $gg \to A, H \to \tau\tau$ cross sections at the LHC at any given m_A. For low $\tan\beta \sim 1$, this lower bound is still of order 0.1 fb for $m_A \sim 500$ GeV, a level that we deem likely to be observable at the LHC during Run 2. For high $\tan\beta$, the lower bound is roughly 2 orders of magnitude higher and only falls below the 0.1 fb level for $m_{A,H} \gtrsim 1.2$ TeV, which is already in the decoupling region. Moreover, while in Type I gluon-gluon fusion is always dominant for H or A production, in Type II, both $b\bar{b}$ associated production and gluon-gluon fusion modes are in principle important since either can be dominant in different regions of the parameter space.

(6) Higgs-to-Higgs decays of the non-SM-like states ($A \to ZH$, $H \to ZA$, $H \to AA$) also open intriguing possibilities for testing the regime of alignment without decoupling, with cross sections often in the range of 1–10 pb (although they can also be quite suppressed). Particularly promising are $gg \to H \to ZA$ and $gg \to H \to AA$ in Type II for light pseudoscalars below about 100 GeV; for such a light A, m_H can be at most ~650 GeV, and $\sigma \times \mathcal{B}$ values for these channels typically range from 10 fb to 10 pb.

In short, it is possible that the observed 125 GeV Higgs boson appears SM-like due to the alignment limit of a multidoublet Higgs sector. The alignment limit does not necessarily imply that the additional Higgs states of the model are heavy. Indeed, they can be light and non-decoupled and thus lead to exciting new effects to be probed at Run 2 of the LHC.

ACKNOWLEDGMENTS

J. B. and S. K. thank Jose Miguel No and Ken Mimasu for discussions on the $A \to ZH$ decay during the “Physics at TeV Colliders” workshop in Les Houches June 10–19, 2015. This work was supported in part by the Research Executive Agency of the European Union under Grant No. PITN-GA2012-316704 (HiggsTools) and by the “Investissements d’avenir, Labex ENIGMASS.” H. E. H. is supported in part by U.S. Department of Energy Grant No. DE-FG02-04ER41286. J. F. G. and Y. J. are supported in part by the U.S. DOE Grant No. DE-SC-000999. Y. J. also acknowledges support by the LHC-TI fellowship US NSF Grant No. PHY-0969510, and he thanks the LPSC Grenoble for its hospitality. J. F. G., H. E. H., and S. K. are grateful for the hospitality and the inspiring working atmosphere of the Aspen Center for Physics, supported by the National Science Foundation Grant No. PHY-1066293, where this project was initiated.

APPENDIX A: SCALAR POTENTIAL QUARTIC COEFFICIENTS IN THE $\mathbb{Z}_2$-BASIS IN TERMS OF HIGGS BASIS COEFFICIENTS

In Eqs. (21)–(25), we have provided expressions for the Higgs basis quantities Z_i in terms of the quartic coefficients of the scalar potential λ_i defined in Eq. (1). In this Appendix, we provide the inverse of Eqs. (21)–(25) by expressing the λ_i in terms of the Z_i,

$$\lambda_1 = Z_1 c_\beta^4 + Z_2 s_\beta^4 + \frac{1}{2} Z_{345} s_{2\beta}^2 - 2 s_{2\beta}(c_\beta^2 Z_6 + s_\beta^2 Z_7), \tag{A1}$$

$$\lambda_2 = Z_1 s_\beta^4 + Z_2 c_\beta^4 + \frac{1}{2} Z_{345} s_{2\beta}^2 + 2 s_{2\beta}(s_\beta^2 Z_6 + c_\beta^2 Z_7), \tag{A2}$$

$$\lambda_i = Z_i + \frac{1}{4} s_{2\beta}^2 (Z_1 + Z_2 - 2Z_{345}) + s_{2\beta} c_{2\beta}(Z_6 - Z_7), \quad \text{for } i = 3, 4, 5, \tag{A3}$$

where $Z_{345} \equiv Z_3 + Z_4 + Z_5$. However, these results do not take into account the fact that $\lambda_6 = \lambda_7 = 0$, which yields two relations among the Z_i. These relations were given in Eqs. (26) and (27) and are repeated below for the convenience of the reader. Recall that we employ a convention where $0 \le \beta \le \frac{1}{2}\pi$. Then, Z_2 and Z_{345} are dependent quantities for $\beta \neq 0, \frac{1}{4}\pi, \frac{1}{2}\pi$,

$$Z_2 = Z_1 + 2(Z_6 + Z_7)\cot 2\beta, \tag{A4}$$

$$Z_{345} = Z_1 + 2Z_6 \cot 2\beta - (Z_6 - Z_7)\tan 2\beta. \tag{A5}$$

An alternative form of Eq. (A5) is obtained by combining the results of Eqs. (A4) and (A5), which yields

$$Z_{345} = Z_2 - 2Z_7 \cot 2\beta - (Z_6 - Z_7)\tan 2\beta. \tag{A6}$$

Taking the average of Eqs. (A5) and (A6) provides one more useful relation that can be used as the second condition for the softly broken $\mathbb{Z}_2$ symmetry along with Eq. (A4),

$$Z_{345} = \frac{1}{2}(Z_1 + Z_2) + 2(Z_6 - Z_7)\cot 4\beta. \quad \text{(A7)}$$

Using Eqs. (A4) and (A7), it follows that if $\beta = 0, \frac{1}{2}\pi$ then $Z_6 = Z_7 = 0$; if $\beta = \frac{1}{8}\pi, \frac{3}{8}\pi$ then $Z_{345} = \frac{1}{2}(Z_1 + Z_2)$; and if $\beta = \frac{1}{4}\pi$ then $Z_1 = Z_2$ and $Z_6 = Z_7$.

Consequently, the expressions for the λ_i in terms of the Z_i can be written in numerous equivalent ways depending on the choice of independent quantities. For example, if $\beta \neq \frac{1}{4}\pi$, then eliminating Z_{345} and either Z_1 or Z_2 yields

$$\lambda_1 = \begin{cases} Z_1 - Z_6 \tan 2\beta + \frac{1}{2}\tan^2\beta \tan 2\beta (Z_6 + Z_7), & \text{if } \beta \neq \frac{1}{2}\pi, \\ Z_2 + Z_7 \tan 2\beta - \frac{1}{2}\cot^2\beta \tan 2\beta (Z_6 + Z_7), & \text{if } \beta \neq 0, \end{cases} \quad \text{(A8)}$$

$$\lambda_2 = \begin{cases} Z_1 - Z_6 \tan 2\beta + \frac{1}{2}\cot^2\beta \tan 2\beta (Z_6 + Z_7), & \text{if } \beta \neq 0, \\ Z_2 + Z_7 \tan 2\beta - \frac{1}{2}\tan^2\beta \tan 2\beta (Z_6 + Z_7), & \text{if } \beta \neq \frac{1}{2}\pi, \end{cases} \quad \text{(A9)}$$

$$\lambda_i = Z_i + \frac{1}{2}(Z_6 - Z_7)\tan 2\beta, \quad \text{for } i = 3, 4, 5. \quad \text{(A10)}$$

Note that the $\mathbb{Z}_2$-basis and the Higgs basis coincide if $\beta = 0$ (in which case $\Phi_1 = H_1$ and $\Phi_2 = H_2$) and if $\beta = \frac{1}{2}\pi$ (in which case $\Phi_1 = H_2$ and $\Phi_2 = H_1$). The two alternative forms given in Eqs. (A8) and (A9) are a consequence of the symmetry of Eqs. (A4)–(A7) under the interchanges, $Z_1 \leftrightarrow Z_2$, $Z_6 \leftrightarrow Z_7$, $\beta \leftrightarrow \frac{1}{2}\pi - \beta$.

The exclusion of $\beta = \frac{1}{4}\pi$ in Eqs. (A8)–(A10) is an artifact of expressing these results in terms of both Z_6 and Z_7. Nevertheless, there is no discontinuity, since $Z_6 = Z_7$ at $\beta = \frac{1}{4}\pi$. One way to avoid this inconvenience is to eliminate either Z_6 or Z_7 in favor of Z_{345}. The end result is

$$\lambda_1 = \begin{cases} Z_1(1 - \frac{1}{2}\tan^2\beta) + \frac{1}{2}Z_{345}\tan^2\beta - \frac{1}{2}Z_6 \tan\beta(5 - \tan^2\beta), & \text{if } \beta \neq \frac{1}{2}\pi, \\ Z_2(1 - \frac{1}{2}\cot^2\beta) + \frac{1}{2}Z_{345}\cot^2\beta - \frac{1}{2}Z_7 \cot\beta(5 - \cot^2\beta), & \text{if } \beta \neq 0, \end{cases} \quad \text{(A11)}$$

$$\lambda_2 = \begin{cases} Z_1(1 - \frac{1}{2}\cot^2\beta) + \frac{1}{2}Z_{345}\cot^2\beta + \frac{1}{2}Z_6 \cot\beta(5 - \cot^2\beta), & \text{if } \beta \neq 0, \\ Z_2(1 - \frac{1}{2}\tan^2\beta) + \frac{1}{2}Z_{345}\tan^2\beta + \frac{1}{2}Z_7 \tan\beta(5 - \tan^2\beta), & \text{if } \beta \neq \frac{1}{2}\pi, \end{cases} \quad \text{(A12)}$$

$$\lambda_i = \begin{cases} Z_i + \frac{1}{2}(Z_1 - Z_{345}) + Z_6 \cot 2\beta, & \text{for } i = 3,4,5 \text{ and } \beta \neq 0, \frac{1}{2}\pi, \\ Z_i + \frac{1}{2}(Z_2 - Z_{345}) - Z_7 \cot 2\beta, & \text{for } i = 3,4,5 \text{ and } \beta \neq 0, \frac{1}{2}\pi. \end{cases} \quad \text{(A13)}$$

Finally, one may choose to eliminate both Z_6 and Z_7, using Eqs. (A4) and (A7). The end result is valid for $\beta \neq \frac{1}{8}\pi, \frac{1}{4}\pi, \frac{3}{8}\pi$,[22]

$$\lambda_1 = \frac{1}{2}(Z_1 + Z_2) + \frac{s_{2\beta}^2}{4c_{4\beta}}(Z_1 + Z_2 - 2Z_{345}) + \frac{1}{2c_{2\beta}}(Z_1 - Z_2), \quad \text{(A14)}$$

$$\lambda_2 = \frac{1}{2}(Z_1 + Z_2) + \frac{s_{2\beta}^2}{4c_{4\beta}}(Z_1 + Z_2 - 2Z_{345}) - \frac{1}{2c_{2\beta}}(Z_1 - Z_2), \quad \text{(A15)}$$

$$\lambda_i = Z_i - \frac{s_{2\beta}^2}{2c_{4\beta}}(Z_1 + Z_2 - 2Z_{345}), \quad \text{for } i = 3, 4, 5. \quad \text{(A16)}$$

The conditions for the stability of the scalar potential [Eq. (1)] for $\lambda_6 = \lambda_7 = 0$ were first given in Ref. [57],

$$\lambda_1 > 0, \qquad \lambda_2 > 0, \qquad \lambda_3 > -\sqrt{\lambda_1\lambda_2}, \\ \lambda_3 + \lambda_4 - |\lambda_5| > -\sqrt{\lambda_1\lambda_2}. \quad \text{(A17)}$$

Using the results of this Appendix, one can rewrite the stability conditions in terms of the Z_i. The resulting expressions are not especially illuminating, so we will not exhibit them explicitly.

In addition, we note that (under the assumption of $\lambda_6 = \lambda_7 = 0$) the λ_i $(i = 1, 2, \ldots, 5)$ can be reconstructed in principle as follows. Assume that $c_{\beta-\alpha}$ has been deduced from precision measurements of the SM-like Higgs boson (assumed to be h) and β is determined via the properties of

[22]Eliminating both Z_6 and Z_7 is not particularly useful in the cases of $\beta = \frac{1}{8}\pi, \frac{3}{8}\pi$, where $Z_1 + Z_2 = 2Z_{345}$ and in the case of $\beta = \frac{1}{4}\pi$, where $Z_1 = Z_2$ [cf. Eqs. (A4) and (A7)].

the heavier Higgs states. We also assume that all four Higgs masses (m_h, m_H, m_A, and $m_{H^\pm}$) have been measured. Lastly, we assume that a small deviation in the signal strength for $h \to \gamma\gamma$ can be attributed to the presence of a charged Higgs loop,[23] in which case we can extract a value for $g_{hH^+H^-}$. With all this information in hand, we begin by using Eq. (47) [or equivalently, Eq. (42)] to obtain Z_6. Next, we employ Eqs. (41) and (43) to obtain Z_1 and Z_5 and Eqs. (33) and (34) for the squared-mass difference, $m^2_{H^\pm} - m^2_A$, to deduce $Z_4 - Z_5$, which together with the previous determination yields a value for Z_4. Close to the alignment limit, we can use $g_{hH^+H^-}$ to extract Z_3 [cf. Eqs. (65) and (76)]. We now have enough information to evaluate Z_{345}. Finally, we can use Eqs. (A9) and (A10) to obtain Z_2 and Z_7. We now have all the Z_i (for $i = 1, 2, \ldots 7$), which can then be employed with the formulas provided in this Appendix to obtain the λ_i ($i = 1, 2, \ldots, 5$).

APPENDIX B: TRILINEAR HIGGS SELF-COUPLINGS IN TERMS OF PHYSICAL HIGGS MASSES

It is convenient to reexpress the trilinear Higgs self-couplings in terms of the physical Higgs masses. First, Eqs. (32) and (34) yield

$$(Z_3 + Z_4 - Z_5)v^2 = 2(m^2_A - \bar{m}^2) + Z_1 v^2 + 2Z_6 v^2 \cot 2\beta. \tag{B1}$$

Using this result along with Eqs. (41)–(43) and (49), we end up with

$$\begin{aligned}&[(Z_3 + Z_4 - Z_5)s_{\beta-\alpha} + Z_7 c_{\beta-\alpha}]v^2 \\ &\quad = [m^2_h + 2(m^2_A - \bar{m}^2)]s_{\beta-\alpha} + 2\cot 2\beta(m^2_h - \bar{m}^2)c_{\beta-\alpha},\end{aligned} \tag{B2}$$

$$\begin{aligned}&[(Z_3 + Z_4 - Z_5)c_{\beta-\alpha} - Z_7 s_{\beta-\alpha}]v^2 \\ &\quad = [m^2_H + 2(m^2_A - \bar{m}^2)]c_{\beta-\alpha} - 2\cot 2\beta(m^2_H - \bar{m}^2)s_{\beta-\alpha}.\end{aligned} \tag{B3}$$

Noting that Eqs. (33) and (34) yield $m^2_A - m^2_{H^\pm} = \frac{1}{2}(Z_4 - Z_5)v^2$, the above results immediately yield

$$\begin{aligned}&[Z_3 s_{\beta-\alpha} + Z_7 c_{\beta-\alpha}]v^2 \\ &\quad = [m^2_h + 2(m^2_{H^\pm} - \bar{m}^2)]s_{\beta-\alpha} + 2\cot 2\beta(m^2_h - \bar{m}^2)c_{\beta-\alpha},\end{aligned} \tag{B4}$$

$$\begin{aligned}&[Z_3 c_{\beta-\alpha} - Z_7 s_{\beta-\alpha}]v^2 \\ &\quad = [m^2_H + 2(m^2_{H^\pm} - \bar{m}^2)]c_{\beta-\alpha} - 2\cot 2\beta(m^2_H - \bar{m}^2)s_{\beta-\alpha}.\end{aligned} \tag{B5}$$

Thus, from Eqs. (59)–(66), we obtain

$$\begin{aligned}g_{hAA} = -\frac{1}{v}\{&[m^2_h + 2(m^2_A - \bar{m}^2)]s_{\beta-\alpha} \\ &+ 2\cot 2\beta(m^2_h - \bar{m}^2)c_{\beta-\alpha}\},\end{aligned} \tag{B6}$$

$$\begin{aligned}g_{HAA} = -\frac{1}{v}\{&[m^2_H + 2(m^2_A - \bar{m}^2)]c_{\beta-\alpha} \\ &- 2\cot 2\beta(m^2_H - \bar{m}^2)s_{\beta-\alpha}\},\end{aligned} \tag{B7}$$

$$\begin{aligned}g_{hH^+H^-} = -\frac{1}{v}\{&[m^2_h + 2(m^2_{H^\pm} - \bar{m}^2)]s_{\beta-\alpha} \\ &+ 2\cot 2\beta(m^2_h - \bar{m}^2)c_{\beta-\alpha}\},\end{aligned} \tag{B8}$$

$$\begin{aligned}g_{HH^+H^-} = -\frac{1}{v}\{&[m^2_H + 2(m^2_{H^\pm} - \bar{m}^2)]c_{\beta-\alpha} \\ &- 2\cot 2\beta(m^2_H - \bar{m}^2)s_{\beta-\alpha}\}.\end{aligned} \tag{B9}$$

$$g_{hHH} = \frac{s_{\beta-\alpha}}{v}\{2\bar{m}^2 - 2m^2_H - m^2_h + 2(3\bar{m}^2 - 2m^2_H - m^2_h)(s_{\beta-\alpha}\cot 2\beta - c_{\beta-\alpha})c_{\beta-\alpha}\}, \tag{B10}$$

$$g_{Hhh} = -\frac{c_{\beta-\alpha}}{v}\{4\bar{m}^2 - m^2_H - 2m^2_h + 2(3\bar{m}^2 - m^2_H - 2m^2_h)(s_{\beta-\alpha}\cot 2\beta - c_{\beta-\alpha})c_{\beta-\alpha}\}, \tag{B11}$$

$$g_{hhh} = -\frac{3}{v}\{m^2_h s_{\beta-\alpha} + 2(m^2_h - \bar{m}^2)(c_{\beta-\alpha}\cot 2\beta + s_{\beta-\alpha})c^2_{\beta-\alpha}\}, \tag{B12}$$

$$g_{HHH} = -\frac{3}{v}\{m^2_H c_{\beta-\alpha} - 2(m^2_H - \bar{m}^2)(s_{\beta-\alpha}\cot 2\beta - c_{\beta-\alpha})s^2_{\beta-\alpha}\}, \tag{B13}$$

[23] In the absence of a clear deviation from the SM in the $\gamma\gamma$ signal, one would be forced to seek out some measurable triple Higgs coupling involving no more than a single SM-like Higgs boson to avoid a suppression of the term that is sensitive to Z_3 or Z_7 [cf. Eqs. (59)–(60)].

[1] G. Aad *et al.* (ATLAS Collaboration), Phys. Lett. B **716**, 1 (2012).
[2] S. Chatrchyan *et al.* (CMS Collaboration), Phys. Lett. B **716**, 30 (2012).
[3] G. Aad *et al.* (ATLAS and CMS Collaborations), Phys. Rev. Lett. **114**, 191803 (2015).
[4] ATLAS Collaboration, Tech. Report No. ATLAS-CONF-2015-007, 2015.
[5] V. Khachatryan *et al.* (CMS Collaboration), Eur. Phys. J. C **75**, 212 (2015).
[6] J. Bernon, B. Dumont, and S. Kraml, Phys. Rev. D **90**, 071301 (2014).
[7] P. Fayet, Nucl. Phys. **B90**, 104 (1975).
[8] K. Inoue, A. Kakuto, H. Komatsu, and S. Takeshita, Prog. Theor. Phys. **67**, 1889 (1982).
[9] R. A. Flores and M. Sher, Ann. Phys. (N.Y.) **148**, 95 (1983).
[10] J. Gunion and H. E. Haber, Nucl. Phys. **B272**, 1 (1986).
[11] L. J. Hall and M. B. Wise, Nucl. Phys. **B187**, 397 (1981).
[12] J. F. Gunion and H. E. Haber, Phys. Rev. D **67**, 075019 (2003).
[13] B. Dumont, J. F. Gunion, Y. Jiang, and S. Kraml, Phys. Rev. D **90**, 035021 (2014).
[14] B. Dumont, J. F. Gunion, Y. Jiang, and S. Kraml, arXiv:1409.4088.
[15] B. Coleppa, F. Kling, and S. Su, J. High Energy Phys. 01 (2014) 161.
[16] O. Eberhardt, U. Nierste, and M. Wiebusch, J. High Energy Phys. 07 (2013) 118.
[17] S. Chang, S. K. Kang, J. P. Lee, K. Y. Lee, S. C. Park, and J. Song, J. High Energy Phys. 09 (2014) 101.
[18] K. Cheung, J. S. Lee, and P. Y. Tseng, J. High Energy Phys. 01 (2014) 085.
[19] J. Baglio, O. Eberhardt, U. Nierste, and M. Wiebusch, Phys. Rev. D **90**, 015008 (2014).
[20] D. Chowdhury and O. Eberhardt, arXiv:1503.08216.
[21] N. Craig, F. D'Eramo, P. Draper, S. Thomas, and H. Zhang, J. High Energy Phys. 06 (2015) 137.
[22] H. E. Haber, arXiv:1401.0152.
[23] D. Asner *et al.*, arXiv:1310.0763.
[24] N. Craig, J. Galloway, and S. Thomas, arXiv:1305.2424.
[25] M. Carena, I. Low, N. R. Shah, and C. E. Wagner, J. High Energy Phys. 04 (2014) 015.
[26] M. Carena, H. E. Haber, I. Low, N. R. Shah, and C. E. M. Wagner, Phys. Rev. D **91**, 035003 (2015).
[27] J. Bernon, J. F. Gunion, Y. Jiang, and S. Kraml, Phys. Rev. D **91**, 075019 (2015).
[28] S. Dawson *et al.*, arXiv:1310.8361.
[29] J. Bernon, J. F. Gunion, H. E. Haber, Y. Jiang, and S. Kraml (unpublished).
[30] D. Eriksson, J. Rathsman, and O. Stal, Comput. Phys. Commun. **181**, 189 (2010).
[31] J. Bernon and B. Dumont, arXiv:1502.04138.
[32] R. V. Harlander, S. Liebler, and H. Mantler, Comput. Phys. Commun. **184**, 1605 (2013).
[33] K. Arnold *et al.*, Comput. Phys. Commun. **180**, 1661 (2009).
[34] J. F. Gunion, H. E. Haber, G. L. Kane, and S. Dawson, *The Higgs Hunter's Guide* (Westview Press, Boulder, CO, 2000).
[35] G. Branco *et al.*, Phys. Rep. **516**, 1 (2012).
[36] S. L. Glashow and S. Weinberg, Phys. Rev. D **15**, 1958 (1977).
[37] E. Paschos, Phys. Rev. D **15**, 1966 (1977).
[38] U. Haisch, arXiv:0805.2141.
[39] F. Mahmoudi and O. Stal, Phys. Rev. D **81**, 035016 (2010).
[40] R. S. Gupta and J. D. Wells, Phys. Rev. D **81**, 055012 (2010).
[41] M. Jung, A. Pich, and P. Tuzon, J. High Energy Phys. 11 (2010) 003.
[42] A. Barroso, P. Ferreira, and R. Santos, Phys. Lett. B **632**, 684 (2006).
[43] I. Ivanov, Phys. Rev. D **75**, 035001 (2007).
[44] G. C. Branco, L. Lavoura, and J. P. Silva, *CP Violation* (Oxford University Press, Oxford, England, 1999).
[45] S. Davidson and H. E. Haber, Phys. Rev. D **72**, 035004 (2005).
[46] H. E. Haber and O. Stål, arXiv:1507.04281.
[47] H. E. Haber and D. O'Neil, Phys. Rev. D **74**, 015018 (2006).
[48] M. Aoki, S. Kanemura, K. Tsumura, and K. Yagyu, Phys. Rev. D **80**, 015017 (2009).
[49] V. Weisskopf, Phys. Rev. **56**, 72 (1939).
[50] G. Altarelli, Phys. Scr. **T158**, 014011 (2013).
[51] H. E. Haber, M. J. Herrero, H. E. Logan, S. Peñaranda, S. Rigolin, and D. Temes, Phys. Rev. D **63**, 055004 (2001).
[52] M. Carena, H. E. Haber, H. E. Logan, and S. Mrenna, Phys. Rev. D **65**, 055005 (2002).
[53] P. Ferreira, J. F. Gunion, H. E. Haber, and R. Santos, Phys. Rev. D **89**, 115003 (2014).
[54] P. S. B. Dev and A. Pilaftsis, J. High Energy Phys. 12 (2014) 024.
[55] P. Ferreira, H. E. Haber, and J. P. Silva, Phys. Rev. D **79**, 116004 (2009).
[56] G. 't Hooft, in *The Proceedings of the NATO Advanced Study Institute on Recent Developments in Gauge Theories, Cargese, Corsica, August 26–September 8, 1979*, edited by G. 't Hooft *et al.* (Plenum Press, New York, 1980), pp. 135–157.
[57] N. G. Deshpande and E. Ma, Phys. Rev. D **18**, 2574 (1978).
[58] R. Barbieri, L. J. Hall, and V. S. Rychkov, Phys. Rev. D **74**, 015007 (2006).
[59] P. Ferreira and J. P. Silva, Eur. Phys. J. C **69**, 45 (2010).
[60] G. Abbiendi *et al.* (ALEPH, DELPHI, L3, OPAL, and LEP Colaborations), Eur. Phys. J. C **73**, 2463 (2013).
[61] M. E. Peskin and T. Takeuchi, Phys. Rev. D **46**, 381 (1992).
[62] M. Baak, J. Cúth, J. Haller, A. Hoecker, R. Kogler, K. Mönig, M. Schott, and J. Stelzer, Eur. Phys. J. C **74**, 3046 (2014).
[63] R. Barate *et al.* (LEP Working Group for Higgs Boson Searches, ALEPH, DELPHI, L3, and OPAL Collaborations), Phys. Lett. B **565**, 61 (2003).
[64] G. Abbiendi *et al.* (OPAL Collaboration), Eur. Phys. J. C **40**, 317 (2005).
[65] F. Domingo, U. Ellwanger, E. Fullana, C. Hugonie, and M.-A. Sanchis-Lozano, J. High Energy Phys. 01 (2009) 061.

[66] U. Ellwanger and C. Hugonie, http://www.th.u-psud.fr/NMHDECAY/nmssmtools.html.
[67] S. Chatrchyan *et al.* (CMS Collaboration), Phys. Rev. Lett. **109**, 121801 (2012).
[68] ATLAS Collaboration, Tech. Report No. ATLAS-CONF-2013-013, 2013.
[69] S. Chatrchyan *et al.* (CMS Collaboration), Phys. Rev. D **89**, 092007 (2014).
[70] CMS Collaboration, Tech. Report No. CMS-PAS-HIG-13-014, 2013.
[71] V. Khachatryan *et al.* (CMS Collaboration), arXiv:1504.00936.
[72] G. Aad *et al.* (ATLAS Collaboration), J. High Energy Phys. 11 (2014) 056.
[73] V. Khachatryan *et al.* (CMS Collaboration), J. High Energy Phys. 10 (2014) 160.
[74] G. Aad *et al.* (ATLAS Collaboration), Phys. Lett. B **744**, 163 (2015).
[75] CMS Collaboration, Tech. Report No. CMS-PAS-HIG-14-011, 2014.
[76] CMS Collaboration, Tech. Report No. CMS-PAS-HIG-14-031, 2015.
[77] V. Khachatryan *et al.* (CMS Collaboration), arXiv:1503.04114.
[78] CMS Collaboration, Tech. Report No. CMS-PAS-HIG-15-001, 2015.
[79] G. Aad *et al.* (ATLAS Collaboration), Phys. Rev. D **90**, 095009 (2014).
[80] G. Aad *et al.* (ATLAS Collaboration), Phys. Rev. D **91**, 012006 (2015).
[81] G. Aad *et al.* (ATLAS Collaboration), J. High Energy Phys. 04 (2015) 117.
[82] G. Aad *et al.* (ATLAS Collaboration), J. High Energy Phys. 01 (2015) 069.
[83] G. Aad *et al.* (ATLAS Collaboration), Eur. Phys. J. C **75**, 349 (2015).
[84] ATLAS Collaboration, Tech. Report No. ATLAS-CONF-2015-006, 2015.
[85] G. Aad *et al.* (ATLAS Collaboration), Phys. Rev. Lett. **112**, 201802 (2014).
[86] G. Aad *et al.* (ATLAS Collaboration), Phys. Lett. B **732**, 8 (2014).
[87] G. Aad *et al.* (ATLAS Collaboration), Phys. Lett. B **738**, 68 (2014).
[88] V. Khachatryan *et al.* (CMS Collaboration), Eur. Phys. J. C **74**, 3076 (2014).
[89] S. Chatrchyan *et al.* (CMS Collaboration), J. High Energy Phys. 01 (2014) 096.
[90] S. Chatrchyan *et al.* (CMS Collaboration), J. High Energy Phys. 05 (2014) 104.
[91] S. Chatrchyan *et al.* (CMS Collaboration), Phys. Rev. D **89**, 012003 (2014).
[92] V. Khachatryan *et al.* (CMS Collaboration), J. High Energy Phys. 09 (2014) 087.
[93] V. Khachatryan *et al.* (CMS Collaboration), Eur. Phys. J. C **75**, 251 (2015).
[94] S. Chatrchyan *et al.* (CMS Collaboration), Eur. Phys. J. C **74**, 2980 (2014).
[95] T. Aaltonen *et al.* (CDF and D0 Collaborations), Phys. Rev. D **88**, 052014 (2013).
[96] M. Misiak *et al.*, Phys. Rev. Lett. **114**, 221801 (2015).
[97] G. Bhattacharyya, D. Das, P. B. Pal, and M. N. Rebelo, J. High Energy Phys. 10 (2013) 081.
[98] G. Bhattacharyya and D. Das, Phys. Rev. D **91**, 015005 (2015).
[99] A. Arhrib, P. M. Ferreira, and R. Santos, J. High Energy Phys. 03 (2014) 053.
[100] G. Dorsch, S. Huber, K. Mimasu, and J. No, Phys. Rev. Lett. **113**, 211802 (2014).
[101] B. Coleppa, F. Kling, and S. Su, J. High Energy Phys. 09 (2014) 161.